iScience

CellPress
OPEN ACCESS

Article

Targeted delivery of immune-stimulating bispecific RNA, inducing apoptosis and anti-tumor immunity in cancer cells

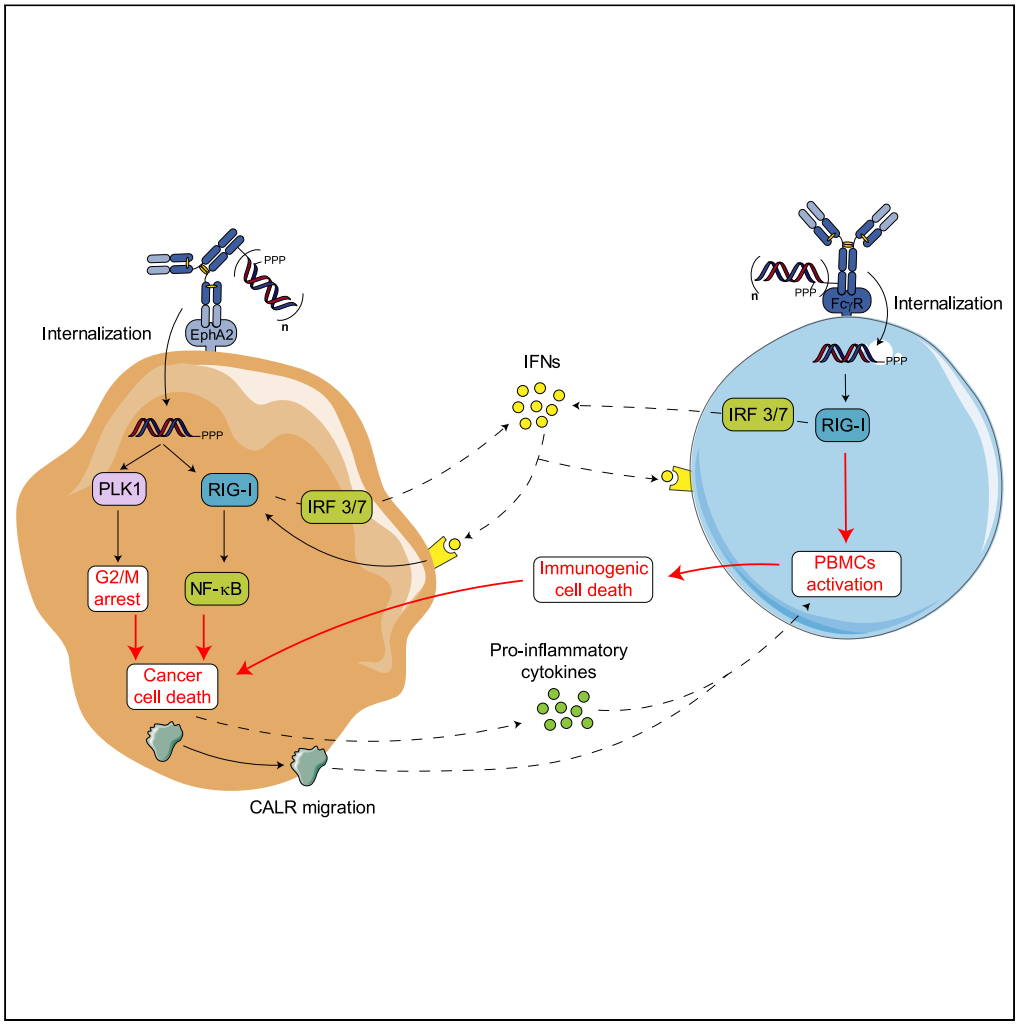

Tony Rady, Stéphane Erb, Safia Deddouche-Grass, ..., Sarah Cianférani, Nicolas Basse, Alain Wagner

nicolas.basse@sanofi.com (N.B.)
alwag@unistra.fr (A.W.)

Highlights

Reliable protocol for antibody-siRNA generation and analysis

Simultaneous RIG-I activation and PLK1 knockdown using a single antibody-siRNA molecule

ARC 1 treatment led to strong anti-tumor pro-inflammatory response with PBMCs

Rady et al., iScience 27, 109068
March 15, 2024 © 2024
https://doi.org/10.1016/j.isci.2024.109068

iScience

CellPress
OPEN ACCESS

Article

Targeted delivery of immune-stimulating bispecific RNA, inducing apoptosis and anti-tumor immunity in cancer cells

Tony Rady,[1,2,5] Stéphane Erb,[3,4] Safia Deddouche-Grass,[2] Renaud Morales,[2] Guilhem Chaubet,[1] Sarah Cianférani,[3,4] Nicolas Basse,[2,*] and Alain Wagner[1,6,*]

SUMMARY

Double-stranded RNAs (dsRNA)-based strategies appeared as promising therapies to induce an inflammation in the tumor microenvironment. However, currently described systems generally lack active targeting of tissues, and their clinical translation is thus limited to intratumoral injection. Herein, we developed an antibody-siRNA-5′triphosphate conjugate with multiple modes of action, combining cell surface EphA2-specific internalization, leading to a simultaneous gene silencing and activation of the receptor retinoic acid-inducible gene I (RIG-I). Recognition of cytosolic siRNA-5′triphosphate by RIG-I triggers the expression of interferons and pro-inflammatory cytokines, inducing an inflammation of the tumor environment and activating neighboring immune cells. In addition, these RIG-I-specific effects synergized with siRNA-mediated PLK1 silencing to promote cancer cell death by apoptosis. Altogether, such immune-stimulating antibody-RNA conjugate opens a novel modality to overcome some limitations encountered by dsRNA molecules currently in clinical trials.

INTRODUCTION

Exploiting the immune system to induce a tumor regression is among the most recent and innovative approaches to fight cancer.[1] It has been made possible by pioneering new therapeutic modalities, such as cellular therapies,[2] bispecific antibodies,[3] or small molecules drugs that promotes a localized inflammation in the tumor microenvironment.[4] Recently, another promising therapeutic strategy to induce an immune response based on using double-stranded RNAs (dsRNA) able to activate ubiquitous proteins called pattern-recognition receptors (PRR) with a high degree of selectivity and of sensitivity was described.[5]

In particular, MK-4621 is a synthetic dsRNA that was administered intratumorally to patients with advanced tumors. This oligonucleotide selectively activates the PRR retinoic acid-inducible gene I (RIG-I), a cytosolic sensor that detects the presence of short,[6] blunt-ended,[7] and base-paired dsRNA[8] ending with either a 5′triphosphate (5′-ppp)[9] or a 5′diphosphate group.[10] Upon binding, RIG-I undergoes conformational changes allowing the interaction with the mitochondrial antiviral-signaling protein (MAVS), which initiates a signaling cascade activating both NF-κB and inteferon regulatory factors (IRF) 3/7 pathways, leading to pro-inflammatory cytokines and type-I interferon (IFN) secretion, respectively (Figure 1).[11–13] However, this drug candidate only showed a moderate efficiency to induce a tumor regression, highlighting the necessity to enhance its potency.[14]

Stronger therapeutic effects were reached by targeting multiple PRRs simultaneously, BO-112,[15] a polymeric dsRNA mimic not only activating RIG-I, but also TLR3 and MDA5. While this candidate elicited good results in clinical phase II,[16] it was also administered intratumorally. There are currently major challenges for the clinical implementation of intratumoral injections of immunotherapies, such as the injectability. Indeed, choosing the tumor sites or even the needle used can impact the clinical trial. Thus, clinical translation of these promising therapies can be hampered by their inefficient delivery. To overcome this limitation, a novel approach eliciting better biodistribution properties is highly required to allow the selective delivery of immune-stimulating dsRNAs to tumors.

In this context, we envisioned to build an immune-stimulating antibody-RNA conjugate (ARC) able to specifically target cancer cell and acting via a multispecific mode of action while allowing intravenous administration to patients.

Regarding tumor homing, we selected an antibody binding to EphA2, a *trans*-membrane tyrosine kinase receptor overexpressed in several cancers and associated with shorter overall survival in patients.[17] In healthy tissues, and upon binding to its ligands, EphA2 is phosphorylated,

[1]Bio-Functional Chemistry (UMR 7199), LabEx Medalis, University of Strasbourg, 74 Route du Rhin, 67400 Illkirch-Graffenstaden, France
[2]Sanofi, 13 Quai Jules Guesde, 94400 Vitry-sur-Seine, France
[3]Laboratoire de Spectrométrie de Masse BioOrganique (LSMBO), Université de Strasbourg, CNRS, IPHC UMR 7178, 67000 Strasbourg, France
[4]Infrastructure Nationale de Protéomique ProFI – FR2048, 67087 Strasbourg, France
[5]Senior author
[6]Lead contact
*Correspondence: nicolas.basse@sanofi.com (N.B.), alwag@unistra.fr (A.W.)
https://doi.org/10.1016/j.isci.2024.109068

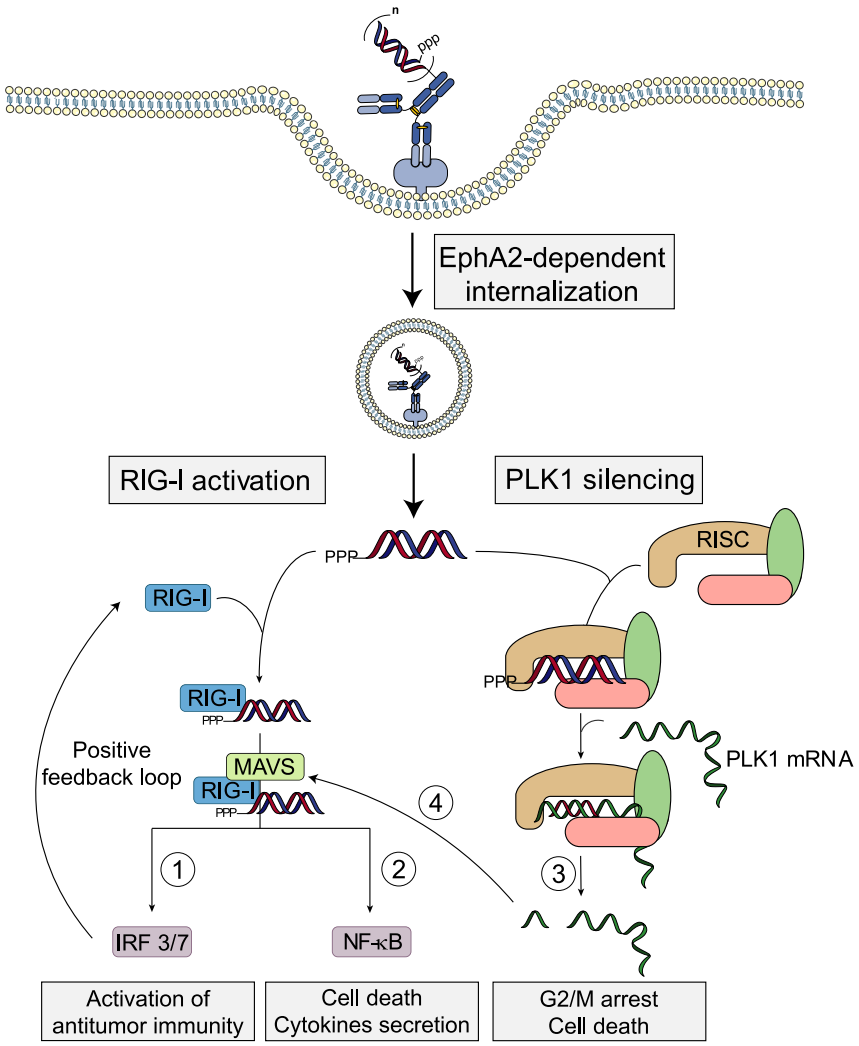

Figure 1. Schematic dual mode of action of antibody-siRNA-5′ppp conjugate

If delivered in the cytosol, the siRNA-5′ppp can be recognized by RIG-I, leading to the activation of both IRF 3/7 (1) and NF-kB (2) signaling pathways, respectively inducing cancer-selective apoptosis, and activating anti-tumor immunity. Concomitantly, the same construct can be loaded in RISC, guiding it to a sequence-complementary mRNA, triggering its degradation (3). In our postulate, silencing PLK1 could lead to the apoptosis by cell-cycle arrest while enhancing MAVS-mediated production of interferon (4).

internalized, and rapidly degraded. However, in cancer cells, this protein-ligand interaction is limited, leading to an accumulation of EphA2 at the plasma membrane and resulting in oncogenic signaling.[18] To address this issue, EphA2 can then be rapidly internalized and degraded upon monoclonal antibody binding, preventing its recycling at the cell surface, while maximizing the intracellular concentration of antibody conjugates.[19] Therefore, antibodies targeting EphA2 appears as a compelling carrier for drug[19–21] or oligonucleotide delivery.[22]

For our multi-specific approach, as the first target, we selected RIG-I, which activation results in the apoptosis of the cancer cell and stimulates the immune system by promoting innate and adaptive immune responses against tumors. In addition, the IFN produced upon RIG-I activation also drives a positive feedback loop increasing RIG-I expression level, thus amplifying the response. As the second target, we reasoned that it should ideally potentiate RIG-I's signaling in order to enhance the antitumoral efficacy of the molecule. As RIG-I activation is independent of the dsRNA sequence, siRNA-5′-ppp combining both RIG-I activation with the silencing of key proteins via the siRNA-mediated degradation of their coding mRNA, were previously designed.[23] To include such silencing activity in our system, we selected Polo-like kinase 1 (PLK1), a protein known as an early trigger for G2/M transition and as a negative regulator of the RIG-I pathway.[24,25] Thus, its knockdown would combine both a G2/M arrest—promoting p53-mediated apoptosis—,[26] with an enhanced IFN production upon RIG-I activation.[24] While there are already PLK1 inhibitors in clinical trials, we hypothesized that the dual targeting of RIG-I- and PLK1 by one single siRNA molecule—coined siPLK1-5′-ppp RNA—would create an effective synergy to induce a strong immune response and tumor regression, while avoiding combinatorial strategies (Figure 1).

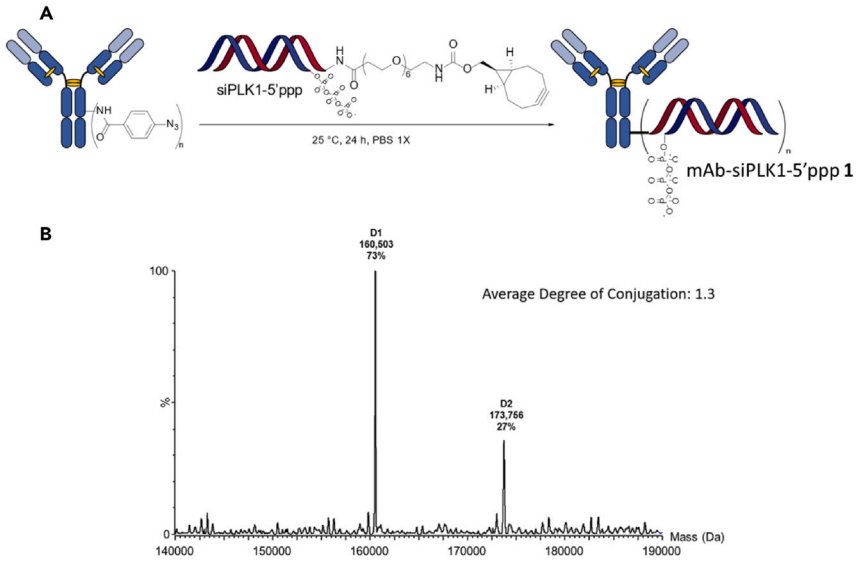

Figure 2. Synthesis scheme and representative analysis of antibody-siRNA conjugate by native SEC-MS

(A) Synthesis of mAb-siRNA-5′ppp 1 and (B) deconvoluted spectra of mAb-siPLK1-5′ppp 1 by native SEC-MS, showing an average degree of conjugation of 1.3. D1 and D2 stand for one and two dsRNA conjugated to the antibody, respectively, with expected D1 being 160,467 Da and expected D2 being 173,769, the naked antibody was discarded during the SEC purification.

RESULTS

Synthesis of the mAb-siPLK1-5′ppp conjugate

The mAb-siPLK-5′ppp conjugate 1 was synthesized in a two-step process relying on straightforward lysine conjugation and click chemistry, as previously described by our laboratory.[27] Briefly, an acyl fluoride first allows the incorporation of an azide group onto the antibody before its derivatization by bio-orthogonal reaction with a strained-alkyne-modified siRNA (Figures 2A and S1).[28] Modification of 3′-amino-RNA was conducted using a short bicyclo[6.1.0]nonyne (BCN)-PEG_6 activated by a pentafluorophenyl ester in basic conditions for 4 h at 25°C. The resulting RNA strand was then hybridized with its complementary strand to afford BCN-siRNA. The latter was then conjugated to the azide-modified anti-EphA2-antibody at 25°C for 24 h, and both unconjugated antibody and the excess of siRNA were removed by size-exclusion chromatography (Figure S3), yielding the desired mAb-siPLK-5′ppp 1 with 41% isolated yield. It should be noted that, in this case, the RIG-I ligand possesses the linker on the 3′ end of the complementary strand, as it was previously shown that RIG-I tolerates non-ribonucleoside modification up to a PEG550.[29]

Regarding the conjugation of the RNA to the antibody, we observed that the click reaction must be conducted after the hybridization with the complementary strand to obtain dsRNA conjugates exclusively. Indeed, when the conjugation was performed before the hybridization, the latter step never reached completion, yielding a mixture of double-stranded and single-stranded ARC (Figures 2B and S4). It should be noticed that only 5′-diphosphate siPLK1 adducts could be detected by native mass spectrometry (MS), due to γ-phosphate fragmentation upon analysis, a common feature of ribonucleotides MS analysis.[30–32]

Intracellular trafficking study by immunofluorescence

In order to investigate the mechanism of delivery, an immunofluorescence study of the intracellular trafficking was engaged by confocal microscopy, allowing to follow independently both the antibody and the siRNA. Accordingly, A549 cells were incubated for different time point with a dual-labeled ARC, composed of a Cy_3-labeled siRNA conjugated to a Cy_5-labeled EphA2-antibody. A fast, antigen-dependent internalization was observed for both dyes after 1 h of incubation at 100 nM (Figures 3A and 3B). As expected, the two dyes were colocalized (Figure S5, Pearson's coefficient = 0.74), suggesting that, at this time point, both biomolecules were still linked and reached lysosomes.

After 4 h of incubation, a separation of the two biomolecules was observed (Figure S5, Pearson's coefficient = 0.18). We observed that this result was in line with the degradation of the EphA2 antibody within 4 h (Figure S6) due to EphA2's biology. Regarding the cytosolic delivery, while the vast majority of intracellular siRNAs colocalized with endo/lysosomes (Pearson's coefficient at 1 h = 0.60, at 4 h = 0.50), a significant portion was still found in the cytosol (Figure 3H). Although both the exact structure of the siRNA that escaped the endosome and the release mechanism itself remain elusive, we hypothesized that the cytosol concentration of siRNA may be sufficient to both activate RIG-I knockdown PLK1.

Characterization of RIG-I signaling activity upon mAb-siPLK1-5′ppp 1 treatment

To evaluate mAb-siPLK1-5′ppp 1 activity *in vitro*, we used the EphA2-positive A549-Dual cell line, engineered to express two reporter genes for both RIG-I signaling pathways (i.e., NF-κB and IRF 3/7). These reporter genes code for an alkaline phosphatase and a luciferase,

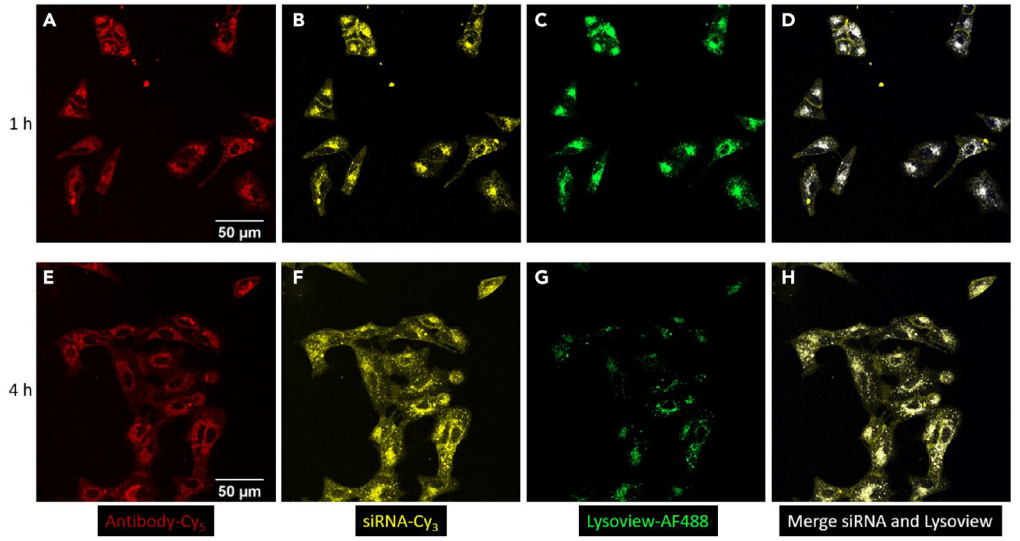

Figure 3. Antibody-siRNA conjugate first colocalize with lysosomes, then siRNA is released in the cytosol

Immunofluorescence pictures obtained from a dual-labeled ARC after 1 h of incubation (A–D, upper line) and 4 h of incubation (E–H, bottom line). Cy5 (red) was conjugated to the antibody's lysines, Cy3 (yellow) was placed at the 5′-end of the siRNA, Lysoview 488 (green, white for the merged pictures) was used to label endo/lysosomes. Pearson's correlation coefficient graphs are provided in the supplemental information in Figure S5.

respectively, whose activities can be quantified to validate RIG-I activation. A RIG-I knock-out (KO) cell line was also used to further validate the RIG-I-dependency.[33]

siPLK1, with or without the 5′ppp moiety, were used either as linker-siRNAs and transfected or conjugated antibodies for all biological experiments performed in this study. Each system was then incubated to A549-Dual and RIG-I KO cell lines for 72 h at 40 nM (Figure 4, see complete figures in Figures S7 and S8). When comparing the activity of 5′-ppp siRNAs with its non-triphosphorylated analogue, we observed that only the former was able to activate both reporter genes in a RIG-I-dependent manner. As expected, transfecting a siPLK1 RNA did not have any influence on RIG-I activation, confirming that the activation of RIG-I is independent of the RNA sequence and rely on the presence of a 5′ triphosphate. After mAb-siPLK1-5′ppp 1 treatment, we observed an activation of both IRF and NF-κB signaling pathways in a dose-dependent manner. No activity could be seen on RIG-I KO cell line, confirming the RIG-I-specific effect, nor using trastuzumab (αHER2 mAb, recycling antigen) as a control ARC, suggesting that the effect on RIG-I might be due to EphA2's biology. In another set of experiments, the cells were first pre-treated with naked anti-EphA2 antibody to induce saturation of EphA2. Following mAb-siPLK1-5′ppp 1 treatment, a decrease in RIG-I activation was observed, demonstrating that the activation was EphA2-dependent (Figure S9). In addition to the immunofluorescence data, these results confirmed that our mAb-siRNA-5′ppp 1 was indeed able to deliver siRNA inside cells in an effective manner and that the latter could be recognized by RIG-I.

mAb-siPLK1-5′ppp 1 simultaneously activates RIG-I and silences PLK1

RIG-I is described to be overexpressed upon activation,[34–36] to confirm this molecular mechanism, its level of expression was measured by western-blot after 72 h of treatment with either 40 nM of mAb-siPLK1-5′ppp 1 or transfected with 40 nM of siPLK1-5′ppp (Figure S10). In comparison with non-treated cells, a 31-fold increase of RIG-I expression was observed with both treatments (Figure 4C), thus confirming the previous RIG-I activation assays. In order to evaluate the dual RIG-I/PLK1 activity, PLK1 expression level was also measured (Figure 4C). As expected, the transfection of siPLK1-5′-ppp could silence about 85% of total PLK1 when compared to untreated cells. The silencing efficiency of the non-triphosphorylated siPLK1 RNA was >95% in the same conditions, this result means that the presence of the triphosphate group has a minimal influence on the silencing efficiency. Under the tested conditions, treatment with mAb-siRNA-5′ppp 1 could silence about 32% of total PLK1, demonstrating that the ARC could perform silencing by RNA interference concomitantly with RIG-I activation. The gene silencing efficiency is, however, lower when the siRNA is delivered by mAb-siPLK1-5′ppp 1, as compared to siRNA lipofection, which is in contrast with the similar efficiencies observed for RIG-I activation. We believe that this difference could be due to the higher amount of cytosolic RNA required to achieve a siRNA effect compared to that needed for RIG-I activation.

As PLK1 knockdown should induce a cell-cycle arrest in the G2/M phase,[26] a cell cycle analysis was performed and the proportion of cells in G2/M phase was quantified by flow cytometry (Figures 4D and S11). 11.6% of non-treated cells were at this phase. A scrambled siRNA control with the 5′triphosphate moiety (siRNA-5′-ppp) gave comparable results, demonstrating that RIG-I activation does not have any influence on the cell cycle. In agreement with the PLK1 expression level following siRNA-mediated knockdown, we determined that 20.4% of the cells were in G2/M phase after transfection of siPLK1 (5′OH or 5′ppp), and 15.3% upon mAb-siPLK1-5′ppp 1 treatment.

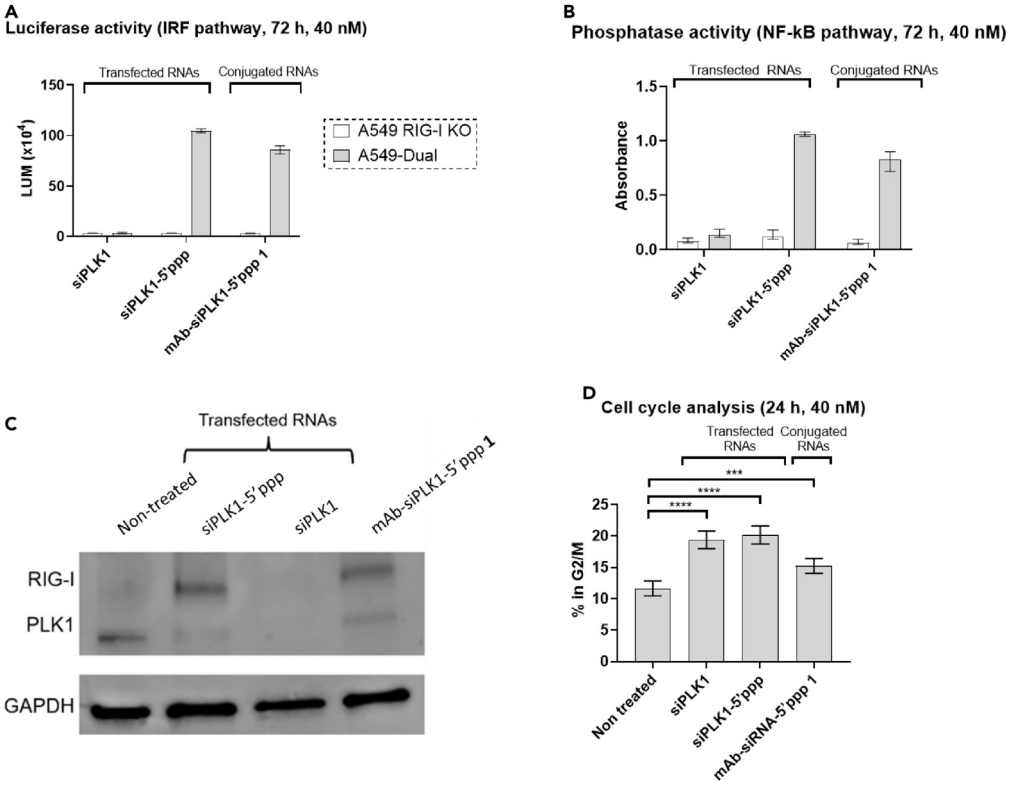

Figure 4. Simultaneous activation of RIG-I and silencing of PLK1 mediated by mAb-siPLK1-5′ppp 1 on A549-Dual

siPLK1-5′ppp was delivered by either RNAiMAX or EphA2-antibody.

(A) RIG-I-dependent activation of the IRF pathway (N = 6, triplicates).

(B) RIG-I-dependent activation of the NF-κB pathway (N = 6, triplicates). Dual activity of the siPLK1-5′ppp delivered by either RNAiMAX or EphA2-antibody regarding RIG-I/PLK1 expression levels or cell-cycle arrest.

(C) Western-blot on RIG-I, PLK1, and GAPDH, showing a simultaneous PLK1 knockdown and RIG-I activation, 72 h after incubation at 40 nM.

(D) Proportion of cells in G2/M phase analyzed by FACS after 24 h of incubation at 40 nM (N = 2, triplicates). Data are presented as mean ± SD. Significancy was assessed by comparing treated cells with non-treated cells, ns = non-significant, *** = $p < 0.0005$, **** = $p < 0.00005$).

mAb-siPLK1-5′ppp 1 induces cancer cell's death by apoptosis and decreases cell proliferation

In order to study further the implication of this dual mode of action for immuno-oncology therapeutic purposes, assays probing cell apoptosis were performed. A WST-1 assay was performed, and after 96 h, we observed a significant decrease in cell viability using both the linker-siPLK1-5′ppp and ARC 1 (Figure S12). Induction of apoptosis by the exposition of phosphatidyl serine and activation of caspase 3/7 was measured using a live-imaging system and profluorescent markers for 96 h.

Regarding the effects of the siRNAs alone, transfections of siPLK1 and siPLK1-5′-ppp strongly induced apoptosis according to both read-outs in A549-Dual cells within 24 h (Figures 5A and S13). This effect is undoubtedly explained by the cell mortality induced by RIG-I-mediated activation and siPLK1-mediated cell-cycle arrest. Unexpectedly, transfection of scrambled versions of these siRNAs also revealed an inhibitory effect on cell proliferation, especially when bearing a 5′ triphosphate end able to activate RIG-I. We did not observe any effect on PLK1 protein using this exact sequence nor any activity using a WST-1 assay, but it is still possible that the siRNA could elicit unexpected off-target effects on other proteins leading to decreased proliferation.

After conjugating the siRNAs to our anti-EphA2-antibody, we repeated these experiments with the resulting conjugates (Figure 5B, video S1). As a negative control, unconjugated anti-EphA2 antibody (yellow line) did not have any influence on the apoptosis nor the confluence of cells. Control siRNAs conjugates (green lines) did not significantly reduce cell confluence over time on both cell lines, showing that the activation on RIG-I alone is not sufficiently potent to induce cell death. In contrast, active siPLK1 (blue lines) drastically decreased cell confluence, showing that most of the killing effect was due to PLK1 silencing. In addition, activation of RIG-I by mAb-siPLK1-5′ppp 1 led to an even greater mortality compared to mAb-siPLK1, suggesting a synergistic effect between RIG-I and PLK1. Overall, while ARCs were less deadly than transfected siRNAs, they were still found to possess potency in the nano-molar range.

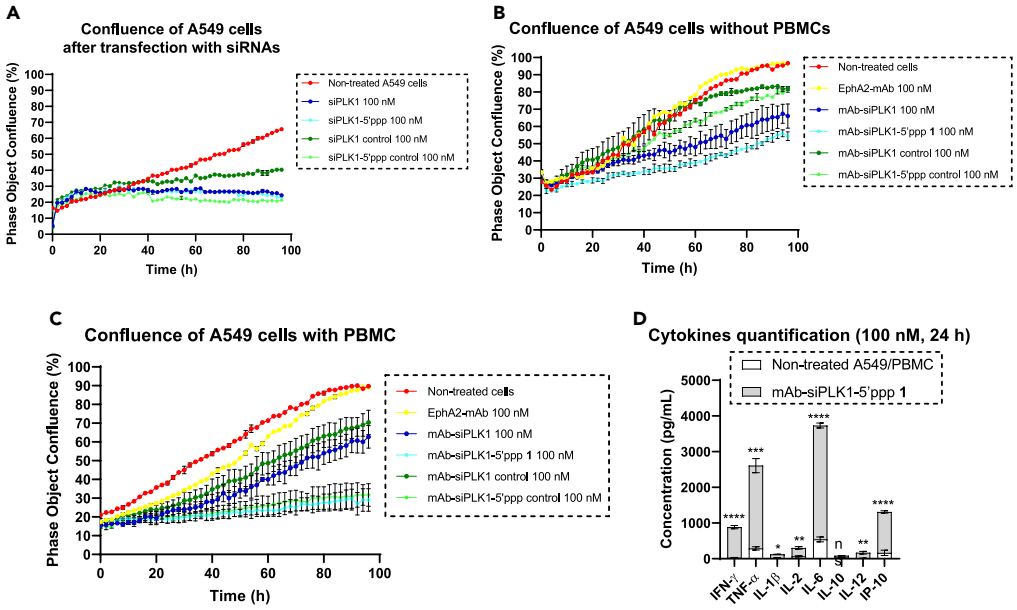

Figure 5. mAb-siPLK1-5′ppp induces A549-Dual cell death by apoptosis and activates PBMCs to promote anti-tumor inflammation

A549-Dual confluence over time after treatments with transfected siRNAs (A) or ARCs (B for A549 cells alone, C for a mixture of A549/PBMC: 1/5). One picture of A549 cells was taken every 2 h for 4 days, PBMC were excluded by the software because of the difference of size between A549 and PBMC, N = 2 with two different donors of PBMCs—(D) Cytokine quantification after mAb-siRNA-5′ppp 1 treatment for 24 h at 100 nM to the A549/PBMC mixture. Data are presented as mean ± SD. Significancy was assessed by comparing the secreted cytokine obtained from mAb-siRNA-5′ppp 1 compared to the non-treated mixture of cells (ns = non-significant, * = $p < 0.05$, ** = $p < 0.005$, *** = $p < 0.0005$, **** = $p < 0.00005$), N = 1, triplicates.

mAb-siPLK1-5′ppp 1 activates PBMCs to perform cancer cell killing

So far, mAb-siPLK1-5′ppp 1 proved to simultaneously activate RIG-I and silence PLK1, thus inducing a cell-cycle arrest and the A549 cells' death by apoptosis. As part of the immunogenic cell death (ICD), mAb-siPLK1-5′ppp 1 proved to be able to release calreticulin (CALR) from treated cells.

In order to determine whether our ARCs could recruit immune cells and induce RIG-I-dependent ICD, experiments with primary peripheral blood mononuclear cells (PBMCs) were conducted under the same conditions. Co-culture experiments with A549 cells and PBMCs (ratio A549/PBMC 1:5) were performed using two different PBMCs donors. Due to the size difference between the PBMC and A549 cells, we were able to monitor selectively the cancer cells by excluding much smaller PBMCs.

It appeared that the cell's confluence was more reduced by RIG-I-activating ARCs (Figure 5C, light green and light blue lines) than by the other ARCs (i.e., not active on RIG-I; dark green and dark blue lines), suggesting that activation of RIG-I appeared more impacting than silencing PLK1 in presence of PBMCs. Furthermore, the cell confluence is significantly reduced when compared to the previous experiment (Figure 5B), suggesting that PBMCs could have been activated in a RIG-I-dependent manner by mAb-siPLK1-5′ppp 1 to perform cancer cell killing. Surprisingly, RIG-I activating ARCs showed similar results regarding cell proliferation on both RIG-I positive and RIG-I KO cell lines (Figure S14). This suggests that ARCs might be able to interact with PBMCs, presumably via Fcγ receptors internalization, leading to RIG-I activation in PBMCs.

In order to confirm RIG-I specific activation of PBMC and to further characterize the immune response induced by mAb-siPLK1-5′ppp 1, a panel of cytokines were quantified by flow cytometry and compared to non-treated cells (Figures 5D and S15; Table S1). As expected, mAb-siPLK1-5′ppp 1 led to the secretion of high levels of IFN-γ (30-fold) and TNF-α (8-fold), highlighting the activation of both IRF-3/7 and NF-kB pathways, respectively. Regarding immune cell recruitment, high levels of IL-2 (3-fold), IL-6 (6-fold), and IL-12 (20-fold) were observed, showing that T cells and dendritic cells were activated by mAb-siPLK1-5′ppp 1, and the absence of IL-10 is in line with these results. Finally, IP-10 was also highly secreted (7-fold), and its effect on immune cell attraction to cancer cells can clearly be observed on video S2. Overall, this secretomic analysis appeared in line with our previous observations that mAb-siPLK1-5′ppp 1 could induce a pro-inflammatory response.

mAb-siPLK1-5′ppp 1 induces the release of calreticulin in A549 cells

RIG-I activation is also described to induce the release of damage-associated molecular patterns (DAMPs), such as CALR, that are able to activate PBMCs.[37] DAMPs are intracellular molecules that are released in the extracellular environment following an inflammatory stress.[38] These molecules can then activate neighboring immune cells, which in turn can kill cancer cells, a mechanism named ICD.[37,39] As an additional readout to the secretion of IP-10, which is considered as a marker for ICD, we thus sought to evaluate whether mAb-siPLK1-5′ppp 1 could induce DAMPs release.

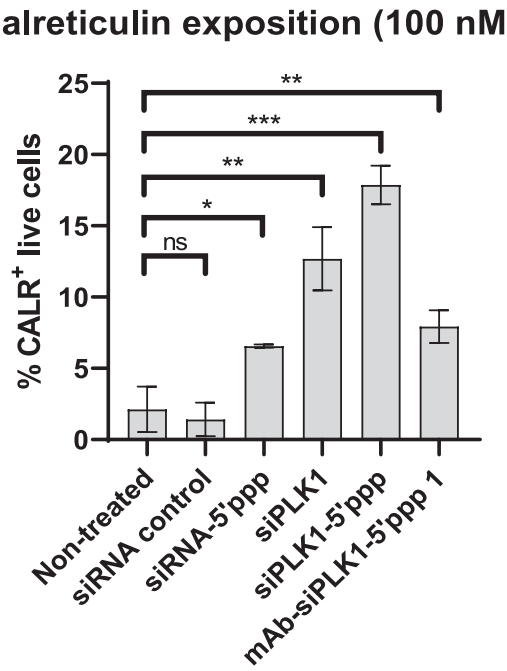

Figure 6. mAb-siPLK1-5′ppp can induce immunogenic cell death

CALR exposition after 48 h of incubation at 100 nM, indicating a possible release of damage-associated molecular patterns (N = 2, triplicates). Data are presented as mean ± SD. Significancy was assessed by comparing treated cells with non-treated cells (ns = non-significant, * = $p < 0.05$, ** = $p < 0.005$, *** = $p < 0.0005$).

To do so, the presence of CALR on the cell surface was assessed by flow cytometry on A549-Dual cells following treatment with either siRNAs or mAb-siPLK1-5′ppp 1 (Figure S15). The proportion of live cells with external CALR was measured, using an AF488-labeled anti-CALR antibody and by labeling dead cells using 7-AAD (Figure 6). As expected, the proportion of $CALR^+$ live cells in non-treated cells (~2.1%) or following transfection of control siRNA was very low (~1.4%). However, 5′-ppp siRNA-transfected cells showed a significant exposition of CALR (~6.6%), confirming that RIG-I activation could release DAMPs. Transfecting the cells with siPLK1 increased this proportion even more significantly (~12.7%), and the presence of a triphosphate moiety on the RNA highlighted a combined effect between PLK1 knockdown and RIG-I activation (~17.9%). mAb-siPLK1-5′ppp 1 led to 7.9%, suggesting that it could also induce the exposition of CALR, though to a lesser degree. Taken together, these results suggest that, in addition to the apoptosis, mAb-siPLK1-5′ppp 1 is also able to induce a slight ICD on cancer cells.

DISCUSSION

Taken together, these results have demonstrated that a dual targeting of RIG-I and PLK1 with an antibody-siRNA conjugate was achievable to induce tumoral cell death as well as immune cell activation. To date, only a few immune stimulating antibody conjugate have been described using either TLR7[40] or TLR9[41] agonists, but never targeting RIG-I using an antibody-siRNA conjugate.

The antibody targeting EphA2 used for tumor specific delivery induced an efficient internalization, as we observed a cytosolic release of the siRNA as evidenced by immunofluorescence studies and functional assays. Indeed, we observed a complete degradation of the antibody within 4 h, which was in lines with the decrease in Pearson's coefficient between the antibody and the siRNA at the same time point. However, the majority of the siRNA remained trapped in endo/lysosome, in accordance with numerous studies, thus limiting the efficiency of the delivery.[42,43] Meanwhile, the decreased colocalization with lysosomes suggests that some siRNA molecules have escaped this organelle and reached the cytosol at the same time. Although not verified, we presume that the structure of the released molecule could be a lysine-linker-siRNA conjugate resulting from the complete antibody degradation, which should not impede the siRNA's machinery nor the recognition by RIG-I.

While most siRNA molecules are usually delivered using stabilized molecules, the challenge with RIG-I is that it requires non-protected sequences, thus endosomal trapping is likely to degrade the RNA. A very limited number of molecules are still able to escape the endosome though, as observed by the numerous FDA-approved tri-GalNAc-siRNA conjugates internalizing by receptor-mediated endocytosis.[44] Such endosomal escape mechanism has been also reported in antibody-mediated delivery studies using non-protected RNA.[44,45] As we hypothesized that similar endosomal escape could be obtained to observe an effect, maximizing the amount of RNA in the lysosomes by targeting a non-recycling antigen was mandatory. Although there is no definitive proof of the mechanism of siRNA endosome escape, many studies have been devoted to it.[46] Dowdy hypothesized that spontaneous, short-lived, small breaches of the endosomal lipid bilayer, which repeatedly occur over time, allow the entry into the cytoplasm proximal to the RNA therapeutic and in proximity to the breach. Alternatively, fusion events

between endosomes, multivesicular bodies, and lysosomes potentially generate a temporary breach of the lipid bilayer, allowing RNA therapeutics to leak into the cytoplasm.[47] Hence, despite that most of the siRNA may have been degraded in the lysosome, we believe that ARC was efficient due to a combination of factors, such as the high sensitivity of RIG-I and the ideal endocytic properties of EphA2. Indeed, we did not observe any activity with a HER2-targeting ARC, suggesting that the drug delivery of ARC can be highly sensitive to the endocytic properties of the targeted antigen, even though we cannot exclude that the expression level difference partially explain our results. Nevertheless, as 5′ppp-dsRNA is an extremely potent RIG-I agonist, one of the key advantages of targeting RIG-I is that a minimal cytosolic delivery of the agonist will induce a self-amplifying signaling loop with high sensitivity. This fact is supported by mAb-siPLK1-5′ppp 1, which proved to be efficient to activate RIG-I and silencing PLK1 in the low nanomolar range, leading to a cell-cycle arrest to the G2/M phase and activation of RIG-I signaling pathway. Cancer cell death was also assessed via this bispecific activity, promoting secretion of CXCL10 and the migration of CALR from the endoplasmic reticulum to the plasma membrane.

Moreover, killing assays with primary immune cells indicated that mAb-siPLK1-5′ppp 1 could induce a Th1 immune response *in vitro* in a RIG-I-dependent manner and leading to the secretion of numerous pro-inflammatory cytokines and chemokines. Unexpectedly, co-culture experiments with RIG-I KO cancer cells showed that mAb-siPLK1-5′ppp 1 was able to activate PBMCs and perform cancer cell killing, suggesting a distinct mechanism of action than previous, relying solely on PBMCs activation. As mAb-siPLK1-5′ppp 1 contains an effective Fc-part, we hypothesize that this conjugate could have been internalized in PBMC, presumably via FcγR-mediated internalization or pinocytosis, leading to the release of the bispecific siRNA in PBMCs.

As siRNA can be recognized by TLRs in the endosomes, we observed that mAb-siPLK1 (lacking the triphosphate moiety) was inducing a strong secretion of pro-inflammatory cytokines on PBMCs only, which cannot be attributed to RIG-I (Table S1; Figure S15). We believe this might be due to TLR7/8 activation, PBMCs being more sensitive to pathogen-associated molecular patterns than endothelial cells. Such finding would support an EphA2-independent internalization in endosomes in PBMCs. Satisfyingly, the RIG-I-activating conjugate was almost systematically a stronger inducer of cytokine secretion than mAb-siPLK1, suggesting that some of the effect on PBMCs is not mediated to TLRs but is likely to be attributed to RIG-I.

Overall, this study demonstrates the potential of ARC for immuno-oncology purposes by expanding the scope of drugs with immune-stimulating RNAs. We have demonstrated that it was possible to observe an activity, even with a non-optimized construct, showing the therapeutic potential of such approach if optimized siRNAs are used. One possibility to circumvent the low stability of RNA molecules while keeping an active targeting may be to use antibody-coated lipid nanoparticles.

Antibody-siRNA conjugates are still a recent modality, however, similar approaches have been used for a variety of indication and very recently a first-in-class ARC has recently entered clinical phase I for myotonic dystrophy type 1,[48] confirming the therapeutic potential of such modality.

Limitations of the study

The main limitation of the study is that we were not able to determine what was the exact mechanism of endosomal escape. Such findings would be important for futures studies and highly beneficial to the field of antibody-oligonucleotide conjugates. Another limit of the study is the expected low plasma stability of the construct due to lack of RNA protecting groups.

STAR★METHODS

Detailed methods are provided in the online version of this paper and include the following:

- KEY RESOURCES TABLE
- RESOURCE AVAILABILITY
  - Lead contact
  - Materials availability
  - Data and code availability
- EXPERIMENTAL MODEL AND STUDY PARTICIPANT DETAILS
  - Cell culture
  - Cell culture for confocal microscopy
- METHOD DETAILS
  - Chemical syntheses
  - Synthesis of BCN-siRNA conjugates
  - mAb-N3 synthesis
  - mAb-siRNA synthesis
  - Dual-labelled-mAb-siRNA conjugate synthesis for confocal microscopy
  - Biological assays
- QUANTIFICATION AND STATISTICAL ANALYSIS

SUPPLEMENTAL INFORMATION

Supplemental information can be found online at https://doi.org/10.1016/j.isci.2024.109068.

ACKNOWLEDGMENTS

This project was funded in the context of a Convention Industrielle de Formation par la Recherche (CIFRE, N° 2018/0786) for a PhD fellowship (T.R.) and has thus received funding from both Sanofi and Agence Nationale de la Recherche de la Technologie (ANRT). This work was supported by the CNRS, the University of Strasbourg, and the French Proteomic Infrastructure (ProFI; ANR-10-INBS-08-03).

AUTHOR CONTRIBUTIONS

Conceptualization, N.B., A.W., T.R., and S.D.G.; methodology, N.B., A.W., T.R., and S.D.G.; investigation, T.R. and S.E.; validation, N.B., A.W., S.D.G., R.M., and S.C.; resources, T.R. and S.E.; writing – original draft, T.R., A.W., N.B., and S.D.G.; writing – review and editing, T.R. and A.W.; visualization, T.R. and S.E.; supervision, A.W., N.B., S.D.G., S.C., and G.C.; project administration, A.W. and N.B.; funding acquisition, A.W. and N.B.

DECLARATION OF INTERESTS

T.R., S.D.G., R.M., and N.B. were employed by Sanofi during this study, and may be still employed and hold shares.

Received: January 26, 2023
Revised: July 18, 2023
Accepted: January 25, 2024
Published: February 2, 2024

REFERENCES

1. Esfahani, K., Roudaia, L., Buhlaiga, N., Del Rincon, S.V., Papneja, N., and Miller, W.H. (2020). A Review of Cancer Immunotherapy: From the Past, to the Present, to the Future. Curr. Oncol. *27*, 87–97. https://doi.org/10.3747/co.27.5223.
2. Sterner, R.C., and Sterner, R.M. (2021). CAR-T cell therapy: current limitations and potential strategies. Blood Cancer J. *11*, 69. https://doi.org/10.1038/s41408-021-00459-7.
3. Jin, S., Sun, Y., Liang, X., Gu, X., Ning, J., Xu, Y., Chen, S., and Pan, L. (2022). Emerging new therapeutic antibody derivatives for cancer treatment. Signal Transduct. Targeted Ther. *7*, 39. https://doi.org/10.1038/s41392-021-00868-x.
4. Adams, J.L., Smothers, J., Srinivasan, R., and Hoos, A. (2015). Big opportunities for small molecules in immuno-oncology. Nat. Rev. Drug Discov. *14*, 603–622. https://doi.org/10.1038/nrd4596.
5. Schlee, M., and Hartmann, G. (2016). Discriminating self from non-self in nucleic acid sensing. Nat. Rev. Immunol. *16*, 566–580. https://doi.org/10.1038/nri.2016.78.
6. Schmidt, A., Schwerd, T., Hamm, W., Hellmuth, J.C., Cui, S., Wenzel, M., Hoffmann, F.S., Michallet, M.-C., Besch, R., Hopfner, K.-P., et al. (2009). 5′-triphosphate RNA requires base-paired structures to activate antiviral signaling via RIG-I. Proc. Natl. Acad. Sci. USA *106*, 12067–12072. https://doi.org/10.1073/pnas.0900971106.
7. Schlee, M., Roth, A., Hornung, V., Hagmann, C.A., Wimmenauer, V., Barchet, W., Coch, C., Janke, M., Mihailovic, A., Wardle, G., et al. (2009). Recognition of 5′ Triphosphate by RIG-I Helicase Requires Short Blunt Double-Stranded RNA as Contained in Panhandle of Negative-Strand Virus. Immunity *31*, 25–34. https://doi.org/10.1016/j.immuni.2009.05.008.
8. Marq, J.-B., Kolakofsky, D., and Garcin, D. (2010). Unpaired 5′ ppp-Nucleotides, as Found in Arenavirus Double-stranded RNA Panhandles, Are Not Recognized by RIG-I. J. Biol. Chem. *285*, 18208–18216. https://doi.org/10.1074/jbc.M109.089425.
9. Hornung, V., Ellegast, J., Kim, S., Brzózka, K., Jung, A., Kato, H., Poeck, H., Akira, S., Conzelmann, K.-K., Schlee, M., et al. (2006). 5′-Triphosphate RNA Is the Ligand for RIG-I. Science *314*, 994–997. https://doi.org/10.1126/science.1132505.
10. Yoneyama, M., Kikuchi, M., Natsukawa, T., Shinobu, N., Imaizumi, T., Miyagishi, M., Taira, K., Akira, S., and Fujita, T. (2004). The RNA helicase RIG-I has an essential function in double-stranded RNA-induced innate antiviral responses. Nat. Immunol. *5*, 730–737. https://doi.org/10.1038/ni1087.
11. Jiang, F., Ramanathan, A., Miller, M.T., Tang, G.-Q., Gale, M., Patel, S.S., and Marcotrigiano, J. (2011). Structural basis of RNA recognition and activation by innate immune receptor RIG-I. Nature *479*, 423–427. https://doi.org/10.1038/nature10537.
12. Wu, Y., Wu, X., Wu, L., Wang, X., and Liu, Z. (2017). The anticancer functions of RIG-I–like receptors, RIG-I and MDA5, and their applications in cancer therapy. Transl. Res. *190*, 51–60. https://doi.org/10.1016/j.trsl.2017.08.004.
13. Chen, X., Qian, Y., Yan, F., Tu, J., Yang, X., Xing, Y., and Chen, Z. (2013). 5′-Triphosphate-siRNA activates RIG-I-dependent type I interferon production and enhances inhibition of hepatitis B virus replication in HepG2.2.15 cells. Eur. J. Pharmacol. *721*, 86–95. https://doi.org/10.1016/j.ejphar.2013.09.050.
14. Moreno, V., Gaudy-Marqueste, C., Wermke, M., Italiano, A., Romano, E., Marabelle, A., Connors, E., Zhou, H., Dobrenkov, K., Chartash, E., et al. (2020). 794 Safety and efficacy results from a phase 1/1b study of intratumoral MK-4621, a retinoic acid-inducible gene I (RIG-I) agonist, plus intravenous pembrolizumab in patients with advanced solid tumors. J. Immunother. Cancer *8*, A842. https://doi.org/10.1136/jitc-2020-SITC2020.0794.
15. Wang, Y., and Yang, S. (2020). Multispecific drugs: the fourth wave of biopharmaceutical innovation. Signal Transduct. Targeted Ther. *5*, 86. https://doi.org/10.1038/s41392-020-0201-3.
16. Marquez Rodas, I., Longo, F., Rodriguez-Ruiz, M., Calles, A., Pérez-Gracia, J., Gomez-Rueda, A., Lopez-Tarruella, S., Ponz-Sarvisé, M., Alvarez, R.M., Soria, A., et al. (2018). Intratumoral BO-112, a double-stranded RNA (dsRNA), alone and in combination with systemic anti-PD-1 in solid tumors. Ann. Oncol. *29*, viii732. https://doi.org/10.1093/annonc/mdy424.049.
17. Tandon, M., Vemula, S.V., and Mittal, S.K. (2011). Emerging strategies for EphA2 receptor targeting for cancer therapeutics. Expert Opin. Ther. Targets *15*, 31–51. https://doi.org/10.1517/14728222.2011.538682.
18. Kullander, K., and Klein, R. (2002). Mechanisms and functions of eph and ephrin signalling. Nat. Rev. Mol. Cell Biol. *3*, 475–486. https://doi.org/10.1038/nrm856.
19. Hasegawa, J., Sue, M., Yamato, M., Ichikawa, J., Ishida, S., Shibutani, T., Kitamura, M., Wada, T., and Agatsuma, T. (2016). Novel anti-EPHA2 antibody, DS-8895a for cancer treatment. Cancer Biol. Ther. *17*, 1158–1167. https://doi.org/10.1080/15384047.2016.1235663.
20. Lee, J.W., Stone, R.L., Lee, S.J., Nam, E.J., Roh, J.W., Nick, A.M., Han, H.D., Shahzad, M.M.K., Kim, H.S., Mangala, L.S., et al. (2010). EphA2 Targeted Chemotherapy Using an Antibody Drug Conjugate in Endometrial Carcinoma. Clin. Cancer Res. *16*, 2562–2570. https://doi.org/10.1158/1078-0432.CCR-10-0017.
21. Jackson, D., Gooya, J., Mao, S., Kinneer, K., Xu, L., Camara, M., Fazenbaker, C., Fleming, R., Swamynathan, S., Meyer, D., et al. (2008). A Human Antibody-Drug Conjugate Targeting EphA2 Inhibits Tumor Growth In vivo. Cancer Res. *68*, 9367–9374. https://doi.org/10.1158/0008-5472.CAN-08-1933.
22. Arnold, A.E., Malek-Adamian, E., Le, P.U., Meng, A., Martínez-Montero, S., Petrecca, K., Damha, M.J., and Shoichet, M.S. (2018). Antibody-Antisense Oligonucleotide Conjugate Downregulates a Key Gene in Glioblastoma Stem Cells. Mol. Ther. Nucleic

Acids *11*, 518–527. https://doi.org/10.1016/j.omtn.2018.04.004.
23. Poeck, H., Besch, R., Maihoefer, C., Renn, M., Tormo, D., Morskaya, S.S., Kirschnek, S., Gaffal, E., Landsberg, J., Hellmuth, J., et al. (2008). 5′-triphosphate-siRNA: turning gene silencing and Rig-I activation against melanoma. Nat. Med. *14*, 1256–1263. https://doi.org/10.1038/nm.1887.
24. Vitour, D., Dabo, S., Ahmadi Pour, M., Vilasco, M., Vidalain, P.-O., Jacob, Y., Mezel-Lemoine, M., Paz, S., Arguello, M., Lin, R., et al. (2009). Polo-like Kinase 1 (PLK1) Regulates Interferon (IFN) Induction by MAVS. J. Biol. Chem. *284*, 21797–21809. https://doi.org/10.1074/jbc.M109.018275.
25. Quicke, K.M., Diamond, M.S., and Suthar, M.S. (2017). Negative regulators of the RIG-I-like receptor signaling pathway. Eur. J. Immunol. *47*, 615–628. https://doi.org/10.1002/eji.201646484.
26. Liu, X., and Erikson, R.L. (2003). Polo-like kinase (Plk)1 depletion induces apoptosis in cancer cells. Proc. Natl. Acad. Sci. USA *100*, 5789–5794. https://doi.org/10.1073/pnas.1031523100.
27. Maruani, A., Smith, M.E.B., Miranda, E., Chester, K.A., Chudasama, V., and Caddick, S. (2015). A plug-and-play approach to antibody-based therapeutics via a chemoselective dual click strategy. Nat. Commun. *6*, 6645. https://doi.org/10.1038/ncomms7645.
28. Dovgan, I., Ursuegui, S., Erb, S., Michel, C., Kolodych, S., Cianférani, S., and Wagner, A. (2017). Acyl Fluorides: Fast, Efficient, and Versatile Lysine-Based Protein Conjugation via Plug-and-Play Strategy. Bioconjugate Chem. *28*, 1452–1457. https://doi.org/10.1021/acs.bioconjchem.7b00141.
29. Palmer, C.R., Jacobson, M.E., Fedorova, O., Pyle, A.M., and Wilson, J.T. (2018). Environmentally Triggerable Retinoic Acid-Inducible Gene I Agonists Using Synthetic Polymer Overhangs. Bioconjugate Chem. *29*, 742–747. https://doi.org/10.1021/acs.bioconjchem.7b00697.
30. Strzelecka, D., Chmielinski, S., Bednarek, S., Jemielity, J., and Kowalska, J. (2017). Analysis of mononucleotides by tandem mass spectrometry: investigation of fragmentation pathways for phosphate- and ribose-modified nucleotide analogues. Sci. Rep. *7*, 8931. https://doi.org/10.1038/s41598-017-09416-6.
31. Grigorenko, B.L., Rogov, A.V., and Nemukhin, A.V. (2006). Mechanism of Triphosphate Hydrolysis in Aqueous Solution: QM/MM Simulations in Water Clusters. J. Phys. Chem. B *110*, 4407–4412. https://doi.org/10.1021/jp056395w.
32. Kirpekar, F., and Krogh, T.N. (2001). RNA fragmentation studied in a matrix-assisted laser desorption/ionisation tandem quadrupole/orthogonal time-of-flight mass spectrometer. Rapid Commun. Mass Spectrom. *15*, 8–14. https://doi.org/10.1002/1097-0231(20010115)15:1<8::AID-RCM185>3.0.CO;2-S.
33. Wu, W., Zhang, W., Duggan, E.S., Booth, J.L., Zou, M.-H., and Metcalf, J.P. (2015). RIG-I and TLR3 are both required for maximum interferon induction by influenza virus in human lung alveolar epithelial cells. Virology *482*, 181–188. https://doi.org/10.1016/j.virol.2015.03.048.
34. Loo, Y.-M., and Gale, M. (2011). Immune Signaling by RIG-I-like Receptors. Immunity *34*, 680–692. https://doi.org/10.1016/j.immuni.2011.05.003.
35. Hayakari, R., Matsumiya, T., Xing, F., Yoshida, H., Hayakari, M., and Imaizumi, T. (2016). Critical Role of IRF-3 in the Direct Regulation of dsRNA-Induced Retinoic Acid-Inducible Gene-I (RIG-I) Expression. PLoS One *11*, e0163520. https://doi.org/10.1371/journal.pone.0163520.
36. Hayakari, R., Matsumiya, T., Xing, F., Imaizumi, T., and Yoshida, H. (2013). Type I IFN-independent RIG-I expression in response to double-stranded RNA (P1399). J. Immunol. *190*, 57.11.
37. Elion, D.L., Jacobson, M.E., Hicks, D.J., Rahman, B., Sanchez, V., Gonzales-Ericsson, P.I., Fedorova, O., Pyle, A.M., Wilson, J.T., and Cook, R.S. (2018). Therapeutically Active RIG-I Agonist Induces Immunogenic Tumor Cell Killing in Breast Cancers. Cancer Res. *78*, 6183–6195. https://doi.org/10.1158/0008-5472.CAN-18-0730.
38. Galluzzi, L., Vitale, I., Aaronson, S.A., Abrams, J.M., Adam, D., Agostinis, P., Alnemri, E.S., Altucci, L., Amelio, I., Andrews, D.W., et al. (2018). Molecular mechanisms of cell death: recommendations of the Nomenclature Committee on Cell Death 2018. Cell Death Differ. *25*, 486–541. https://doi.org/10.1038/s41418-017-0012-4.
39. Duewell, P., Steger, A., Lohr, H., Bourhis, H., Hoelz, H., Kirchleitner, S.V., Stieg, M.R., Grassmann, S., Kobold, S., Siveke, J.T., et al. (2014). RIG-I-like helicases induce immunogenic cell death of pancreatic cancer cells and sensitize tumors toward killing by CD8+ T cells. Cell Death Differ. *21*, 1825–1837. https://doi.org/10.1038/cdd.2014.96.
40. Gadd, A.J.R., Greco, F., Cobb, A.J.A., and Edwards, A.D. (2015). Targeted Activation of Toll-Like Receptors: Conjugation of a Toll-Like Receptor 7 Agonist to a Monoclonal Antibody Maintains Antigen Binding and Specificity. Bioconjugate Chem. *26*, 1743–1752. https://doi.org/10.1021/acs.bioconjchem.5b00302.
41. Corogeanu, D., Zaki, K., Beavil, A.J., Arnold, J.N., and Diebold, S.S. (2023). Antibody conjugates for targeted delivery of Toll-like receptor 9 agonist to the tumor tissue. PLoS One *18*, e0282831. https://doi.org/10.1371/journal.pone.0282831.
42. Cuellar, T.L., Barnes, D., Nelson, C., Tanguay, J., Yu, S.-F., Wen, X., Scales, S.J., Gesch, J., Davis, D., van Brabant Smith, A., et al. (2015). Systematic evaluation of antibody-mediated siRNA delivery using an industrial platform of THIOMAB–siRNA conjugates. Nucleic Acids Res. *43*, 1189–1203. https://doi.org/10.1093/nar/gku1362.
43. Zavoiura, O., Brunner, B., Casteels, P., Zimmermann, L., Ozog, M., Boutton, C., Helms, M.W., Wagenaar, T., Adam, V., Peterka, J., et al. (2021). Nanobody–siRNA Conjugates for Targeted Delivery of siRNA to Cancer Cells. Mol. Pharm. *18*, 1048–1060. https://doi.org/10.1021/acs.molpharmaceut.0c01001.
44. Xia, C.-F., Boado, R.J., and Pardridge, W.M. (2009). Antibody-Mediated Targeting of siRNA via the Human Insulin Receptor Using Avidin−Biotin Technology. Mol. Pharm. *6*, 747–751. https://doi.org/10.1021/mp800194y.
45. Yu, Z., Zhang, X., Pei, X., Cao, W., Ye, J., Wang, J., Sun, L., Yu, F., Wang, J., Li, N., et al. (2021). Antibody-siRNA conjugates (ARCs) using multifunctional peptide as a tumor enzyme cleavable linker mediated effective intracellular delivery of siRNA. Int. J. Pharm. *606*, 120940. https://doi.org/10.1016/j.ijpharm.2021.120940.
46. Dowdy, S.F. (2023). Endosomal escape of RNA therapeutics: How do we solve this rate-limiting problem? RNA *29*, 396–401. https://doi.org/10.1261/rna.079507.122.
47. Dowdy, S.F., Setten, R.L., Cui, X.-S., and Jadhav, S.G. (2022). Delivery of RNA Therapeutics: The Great Endosomal Escape. Nucleic Acid Therapeut. *32*, 361–368. https://doi.org/10.1089/nat.2022.0004.
48. Mullard, A. (2022). Antibody–oligonucleotide conjugates enter the clinic. Nat. Rev. Drug Discov. *21*, 6–8. d41573-021-00213–00215. https://doi.org/10.1038/d41573-021-00213-5.

STAR★METHODS

KEY RESOURCES TABLE

REAGENT or RESOURCE	SOURCE	IDENTIFIER
Antibodies		
EphA2 mAb	Internal (Sanofi)	N/A
mouse mAb anti-GAPDH	invitrogen	MA5-15738; RRID: AB_10977387
mouse mAb anti-PLK1	Abcam	ab17056: RRID: AB_443612
rabbit mAb anti-RIG-I	Cell Signal	3743S: RRID: AB_2269233
goat mAb anti-human-Fc	Merck	I2136: RRID: AB_260147
AF488-tagged anti-CALR mAb	Abcam	ab196158: RRID: AB_2943095
Biological samples		
Frozen human PBMCs isolated from fresh whole blood	Etablissement francais du sang (EFS)	N/A
Chemicals, peptides, and recombinant proteins		
Hoechst 33342	ThermoFisher	62249
Lysoview 488	Biotium	70067
RNAiMAX	Thermo Fisher Scientific	13778075
7-AAD	Miltenyi Biotec	130-111-568
Resiquimod	Invivogen	tlrl-r848
Hexaethylene glycol	Merck	259268-5G
Potassium iodide	Merck	221945-5G
Silver(I) oxide	Merck	226831-1G
p-Toluenesulfonyl chloride	Merck	T35955-250G
Sodium azide	Merck	71289-50G
tert-Butyl acrylate	Merck	327182-100ML
Potassium *tert*-butoxide	Merck	156671-25G
Palladium, 10% on carbon, Type 487	Alfa Aesar	11438700
(1R,8S,9S)-bicyclo[6.1.0]non-4-yn-9-ylmethyl (4-nitrophenyl) carbonate	In-house	N/A
Lithium hydroxide	Merck	920312-100G
Pentafluorophenol	Thermo Fisher	11453047
N-(3-Dimethylaminopropyl)-*N*′-ethylcarbodiimide	Merck	39391-10ML
Tetramethylfluoroformamidinium hexafluorophosphate	Merck	8510900005
4-Azidobenzoic acid	TCI	A0930
Critical commercial assays		
Quanti-LucTM Gold	Invivogen	rep-qlcg5
Quanti-BlueTM	invivogen	rep-qbs
WST-1 assay	Merck	11644807001
MultiCyt Cell Cycle Screening Kit	Sartorius	Custom order
Incucyte Caspase 3/7 Green dye	Sartorius	4440
Incucyte Annexin V Red dye	Sartorius	4641
iQue Qbeads personalized PlexScreen	Sartorius	Custom order

(*Continued on next page*)

Continued

REAGENT or RESOURCE	SOURCE	IDENTIFIER
Experimental models: Cell lines		
A549-Dual	InvivoGen	a549d-nfis
A549-Dual RIG-I KO	InvivoGen	a549d-korigi
Oligonucleotides		
siPLK1 (antisense strand, UAUUUAAGGAGGGUGAUCU)	Eurogentec	Custom order
siPLK1 (sense strand, (5'ppp)-AGAUCACCCUCCUUAAAUA)	Eurogentec	Custom order
siPLK1 scrambled (antisense strand, UUCUCCGAACGUGUCACGU)	Eurogentec	Custom order
siPLK1 scrambled (sense strand, (5'ppp)-ACGUGACACGUUCGGAGAA)	Eurogentec	Custom order
siRNA control 5'ppp	Invitrogen	tlrl-3prnalv-100
siRNA control	Invitrogen	tlrl-3prnac-100
Software and algorithms		
FlowJo	FlowJo	https://www.flowjo.com/solutions/flowjo
iQue ForeCyt	Sartorius	https://www.sartorius.com/en/products/flow-cytometry/flow-cytometry-software
Prism 9.0.0	GraphPad	https://www.graphpad.com/
Incucyte S3	Sartorius	https://www.sartorius.com/en/products/live-cell-imaging-analysis/live-cell-analysis-software/incucyte-s3-software-v2018b
ImageJ	ImageJ	https://imagej.nih.gov/ij/download.html

RESOURCE AVAILABILITY

Lead contact

Lead contact: Further information and reasonable requests for resources and reagents should be directed to the lead contact, Alain Wagner (alwag@unistra.fr).

Materials availability

There are restrictions to the availability of EphA2 antibody and related conjugates due to being an internal asset.

Data and code availability

- All data reported in this paper will be shared by the lead contact (alwag@unistra.fr) upon request.
- This paper does not report original code.
- Any additional information required to reanalyze the data reported in this paper is available from the lead contact (alwag@unistra.fr) upon request.

EXPERIMENTAL MODEL AND STUDY PARTICIPANT DETAILS

Cell culture

A549-Dual and A549-Dual RIG-I KO (InvivoGen, Ref. a549d-nfis or a549d-korigi, San Diego, California, U.S.A.) were cultured with high glucose Dulbecco's Modified Eagles Medium containing 1% GlutaMAX™ (DMEM, Gibco™, ThermoFisher, Ref. 10566016) and supplemented with 10 μg/mL Blasticidin (InvivoGen, Ref. ant-bl-05), 100 μg/mL Zeocin (InvivoGen, Ref. ant-zn-05), 10% v/v heat inactivated Fetal Bovine Serum (FBS, Gibco™, ThermoFisher, Ref. 10099141). Proliferative cultures were incubated at 37°C in a humidified 5% CO_2 incubator and subculture carried out twice a week by washing the cell monolayers with DPBS followed by addition of accutase solution (Gibco™, ThermoFisher, Ref. A1110501) and incubation at 37°C until the cells detached. Accutase was inactivated by the addition of growth medium before seeding $1.0.10^6$ cells into fresh T175 or T75 flasks. Cell numbers and viability were assessed by Trypan Blue staining (Thermo Fisher Scientific, Ref. T10282) using Countess 2 (Invitrogen, Ref. AMQAX1000).

Cell culture for confocal microscopy

For confocal microscopy experiments, A549-Dual cells were cultured in high glucose DMEM without phenol red (Gibco™, ThermoFisher, Ref. 31053028) supplemented with 1% GlutaMAX™ (DMEM, Gibco™, ThermoFisher, Ref. 10566016) and supplemented with 10 μg/mL Blasticidin (InvivoGen, Ref. ant-bl-05), 100 μg/mL Zeocin (InvivoGen, Ref. ant-zn-05), 10% v/v heat inactivated Fetal Bovine Serum (FBS, Gibco™, ThermoFisher, Ref. 10099141).

METHOD DETAILS

All reagents were obtained from commercial sources and used without prior purifications. Dry solvents were obtained from Merck. All reactions were carried out under an atmosphere of argon in flame-dried glassware with magnetic stirring. Analytical thin layer chromatography (TLC) was performed using plates cut from glass sheets (silica gel SIL-G, Macherey-Nagel, Ref. 809013). Visualization was achieved under a 254 or 365 nm UV light and by immersion in an appropriate staining solution. Column chromatography was carried out as "Flash Chromatography" using silica gel G-80, G-40, G-25, G-12 or G-4 (40-63 μm) from Buchi on a Buchi Reveleris X2.

NMR:1H and 13C NMR spectra were recorded at 23°C on Bruker Advance III - 400 MHz / 500 MHz spectrometers. Recorded shifts are reported in parts per million (δ) and calibrated using residual nondeuterated solvent. Data are represented as follows: chemical shift, multiplicity (s = singlet, d = doublet, t = triplet, q = quartet, m = multiplet, br = broad, app = apparent), coupling constant (J, Hz), integration and assignment for 1H NMR data.

Analytical LC-MS analyses were carried out on Waters 2695 separations module equipped with Waters 2487 UV detector, Waters Acquity QDa mass detector and CORTECS, 2.7 μm, C18, 50 x 4.6 mm column. The flow rate was 1 mL/min and the solvent system was composed as follows: solvent A: 0.05% TFA in water; solvent B: acetonitrile. The gradient run was: 0 to 5 min. – 5% to 95% B; 5 to 6 min. – 95% B; 6 to 7 min. – 5% B. Mass detector was operated in positive MS Scan mode with 600°C probe temperature, 1.5 kV capillary voltage and 10 V cone voltage.

High resolution mass spectra (HRMS) were obtained using an Agilent Q-TOF 6520.

IR spectra were recorded in a Thermo-Nicolet FT/IR-380 spectrometer. Spectra were interpreted with OMNIC 9 software and are reporter in cm-1. The abbreviations used are w (weak), m (medium), s (strong).

Concentrations of protein or RNA solutions in DPBS (calcium and magnesium free, Merck, Ref. D8537-6X500ML) were determined by UV absorbance using a NanoDrop spectrophotometer (Thermo Fisher Scientific, Illkirch, France) at 280 nm for proteins and 260 nm for RNA using their respective molar extinction coefficient. The concentration of antibody conjugates was measured using a BCA Protein Assay Kit (Thermo Fisher Scientific, Illkirch, France, Ref. 23225).

Size Exclusion Chromatography hyphenated to non-denaturing Mass Spectrometry (SEC-non denaturing MS): An ACQUITY UPLC H-class system (Waters, Manchester, UK) comprising a quaternary solvent manager, a sample manager cooled at 10°C, a column oven maintained at room temperature and an UV detector operating at 280 nm and 214 nm was coupled to the Synapt G2 HDMS mass spectrometer (Waters, Manchester, UK). A quantity comprised between 10 to 20 μg of sample were loaded on the ACQUITY UPLC Protein BEH SEC column (2.1 × 150 mm, 1.7 μm particle size, 200 Å pore size from Waters, Manchester, UK) using an isocratic elution of 100 mM ammonium acetate (NH_4OAc) at pH 6.9 and at a flow rate of 0.100 mL/min over 6.0 minutes. The Synapt G2 HDMS was operated in positive mode with a capillary voltage of 3.0 kV while sample cone and pressure in the interface region were set to 180 V and 6 mbar, respectively Acquisitions were performed in 1,000–10,000 m/z range with a 1.5 s scan time. The mass spectrometer was calibrated using singly charged ions produced by a 2 g/L solution of cesium iodide (Acros organics, Thermo Fisher Scientific, Waltham, MA USA) in 2-propanol/water (50/50 v/v). Native MS data interpretations were performed using UniDec software.

RNA sequences (5' to 3'):

siPLK1 antisense (Eurogentec): UAUUUAAGGAGGGUGAUCU

siPLK1 sense (Eurogentec): ppp-AGAUCACCCUCCUUAAAUA

siPLK1 scrambled antisense (Eurogentec): UUCUCCGAACGUGUCACGU

siPLK1 scrambled sense (Eurogentec): ACGUGACACGUUCGGAGAA

siRNA control antisense (Invitrogen, tlrl-3prnalv-100 or tlrl-3prnac-100): ppp-GCAUGCGACCUCUGUUUGA

siRNA control sense (Invitrogen, tlrl-3prnalv-100 or tlrl-3prnac-100): CGUACGCUGGAGACAAACU

RNAs were purchased HPLC-purified from Eurogentec or Invitrogen. Every step using RNA were carried out under a PSM cleaned with ethanol and RNaseZap. Upon reception, tubes were centrifuged, then RNAs were suspended in DEPC-treated water to 100 μM (for biological assays) or 1 mM (for conjugation).

Chemical syntheses

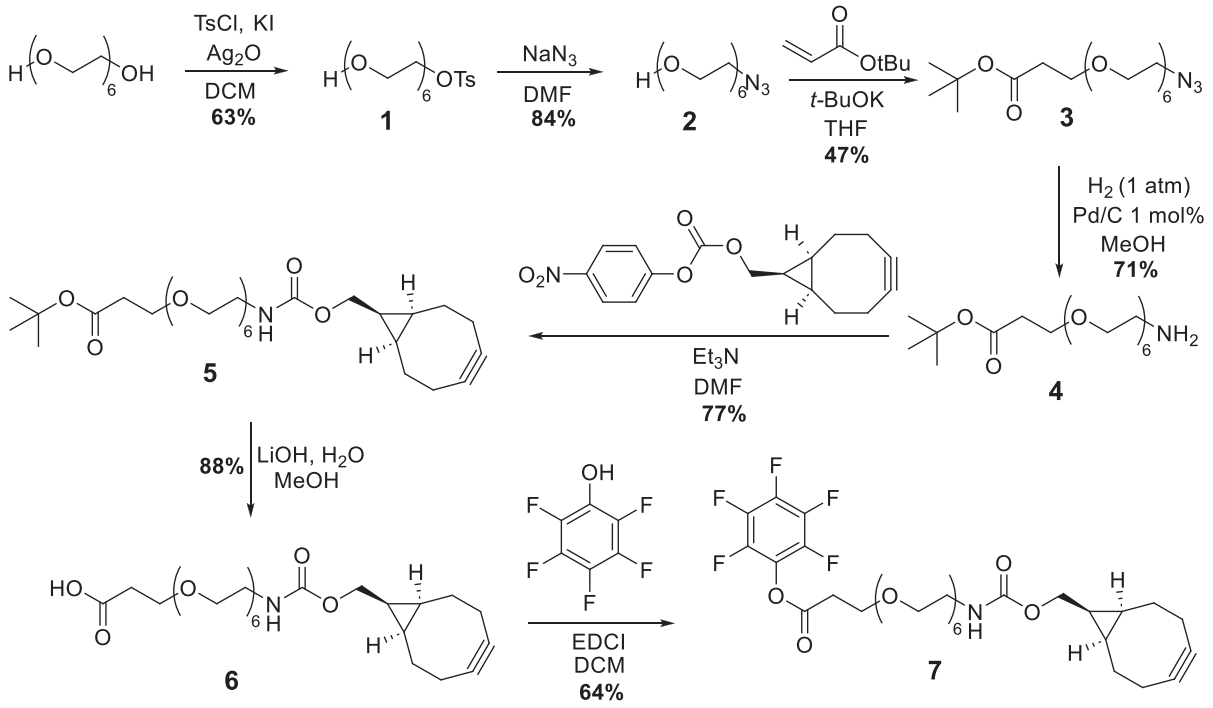

17-hydroxy-3,6,9,12,15-pentaoxaheptadecyl 4-methylbenzenesulfonate 1

To a solution of dried (1 h, 70°C, rotavap) hexaethylene glycol (1 equiv., 20 g, 70.8 mmol) in dichloromethane (320 mL) at 0°C were added KI (0.2 equiv., 2,35 g, 14.2 mmol) and Ag_2O (1.5 equiv., 24,6 g, 106 mmol). Tosyl chloride (1.05 equiv., 14.2 g, 74,4 mmol) was then added portion wise and the reaction mixture was stirred at 0°C for 30 minutes. The mixture was then filtered through a pad of Celite, washed with THF (100 mL) and concentrated in vacuo. The crude material was purified by silica gel flash chromatography (Cyclohexane/EtOAc 85/15 to EtOAc 100% in 5 minutes, then EtOAc 100% for 5 minutes, then EtOAc/MeOH 100/0 to EtOAc/MeOH 95/5 in 20 minutes) to give the title compound **1** as a clear yellow oil (19.3 g, 63%).

^{1}H NMR (400 MHz, $CDCl_3$, δ ppm): 7.78 (d, *J* = 8.2 Hz, 2H), 7.32 (d, *J* = 8.0 Hz, 2H), 4.14(t, *J* = 4.8 Hz, 2H), 3.72–3.53 (m, 22H), 2.94 (s, 1H, (OH)), 2.43 (s, 3H).

^{13}C NMR (100 MHz, $CDCl_3$, δ ppm): 144.8, 133.1, 129.8 (2C), 128.0 (2C), 72.5, 70.7-70.4, 69.7, 68.7, 61.7, 21.6.

17-azido-3,6,9,12,15-pentaoxaheptadecan-1-ol 2

To a solution of 17-hydroxy-3,6,9,12,15-pentaoxaheptadecyl 4-methylbenzenesulfonate **1** (1 equiv., 19.3 g, 44.2 mmol) in DMF (50 mL) was added NaN_3 (1.5 equiv., 4.31 g, 2.33 mL, 66.3 mmol). The reaction was stirred at 50°C overnight under argon atmosphere. After evaporation, 400 mL of dichloromethane were added and the solution was washed with water (1 x 300 mL) then brine (3 x 300 mL). Aqueous layers were combined and washed with dichloromethane (1 x 200 mL) and organic layers were combined, washed with brine (1 x 300 mL), dried over $MgSO_4$, filtered and concentrated in vacuo to afford the title compound **2** as a yellow oil (11.4 g, 37.13 mmol, 84%) which is used without further purifications.

^{1}H NMR (400 MHz, $CDCl_3$, δ ppm): 3.71 – 3.70 (m, 2H), 3.69 – 3.60 (m, 18H), 3.60-3.58 (m, 2H), 3.37 (t, *J* = 5.1 Hz, 2H), 2.98 (s, 1H (OH)).

^{13}C NMR (100 MHz, $CDCl_3$, δ ppm): 72.5, 70.7 – 70.6 (7C), 70.4, 70.0, 61.7, 50.7.

tert-butyl 1-azido-3,6,9,12,15,18-hexaoxahenicosan-21-oate 3

To a solution of 17-azido-3,6,9,12,15-pentaoxaheptadecan-1-ol **2** (1 equiv., 10.5 g, 34.2 mmol) in THF (100 mL, concentration = 0.3 mol/L) at 0°C was added tert-butyl acrylate (1.3 equiv., 5.69 g, 6.45 mL, 44.4 mmol). Freshly sublimated potassium tert-butoxide (0.1 equiv., 0.383 g, 3.42 mmol) was then added portion wise at 0°C and the reaction mixture was stirred at room temperature for 8 h. After concentration, an aqueous solution of NaH_2PO_4 (1M, 100 mL) was added and the mixture was extracted with EtOAc (3 x 200 mL). The combined organic layers

were washed with brine (1 x 200 mL) and dried over $MgSO_4$, filtered and concentrated in vacuo. The crude material was purified by flash chromatography (Cyclohexane/EtOAc 8/2 to EtOAc 100% in 30 minutes) to afford the title compound **3** as a yellow oil (7 g, 16.07 mmol, 47%).

^{1}H NMR (400 MHz, $CDCl_3$, δ ppm): 3.72 - 3.56 (m, 24H), 3.38 (t, 2H), 2.49 (t, 2H), 1.44 (s, 9H).

^{13}C NMR (100 MHz, $CDCl_3$, δ ppm): 171.0, 70.7 – 70.4, 70.1, 66.9, 50.7, 36.3, 28.1 (3C).

tert-butyl 1-amino-3,6,9,12,15,18-hexaoxahenicosan-21-oate 4

To a solution of *tert*-butyl 1-azido-3,6,9,12,15,18-hexaoxahenicosan-21-oate **3** (1 equiv., 1.5 g, 3.44 mmol) in degased methanol (80 mL, concentration under 50 mM) was added Pd/C (1 mol%, 36.7 mg, 34.4 μmol). The atmosphere was flushed with argon then replaced by H_2 and the mixture was stirred at room temperature overnight. The mixture was filtered through a pad of Celite and concentrated *in vacuo*. The crude was purified by silica gel flash chromatography (DCM 100% to DCM/MeOH/NH_4OH 9/0.9/0.1 in 30 minutes) to afford the title compound **4** as a yellow oil (1 g, 2.44 mmol, 71%).

^{1}H NMR (400 MHz, $CDCl_3$, δ ppm): 3.71 – 3.68 (m, 2H), 3.66 – 3.57 (m, 20H), 3.53 – 3.51 (m, 2H), 2.88 – 2.85 (t, 2H), 2.51 – 2.47 (t, 2H), 1.84 (s, 2H (NH_2)), 1.43 (s, 9H).

^{13}C NMR (100 MHz, $CDCl_3$, δ ppm): 170.9, 80.5, 73.1, 70.6 – 70.3, 66.9, 50.7, 41.7, 36.3, 28.1 (3C).

tert-butyl 1-(bicyclo[6.1.0]non-4-yn-9-yl)-3-oxo-2,7,10,13,16,19,22-heptaoxa-4-azapentacosan-25-oate 5

To a solution of (1R,8S,9S)-bicyclo[6.1.0]non-4-yn-9-ylmethyl (4-nitrophenyl) carbonate (1 equiv., 350 mg, 1.11 mmol) in DMF (3 mL) was added a solution of *tert*-butyl 1-amino-3,6,9,12,15,18-hexaoxahenicosan-21-oate **4** (1.1 equiv., 500 mg, 1.22 mmol) and triethylamine (3 equiv., 336 mg, 0.463 mL, 3.33 mmol) in DMF (3 mL). The mixture was stirred overnight at room temperature under argon atmosphere. After concentration, a solution of NaH_2PO_4 (1M, 100 mL) was added and the mixture was extracted with EtOAc (3 x 100 mL). The combined organic layers were washed with brine (100 mL), dried over $MgSO_4$ and concentrated *in vacuo*. The residue was purified by flash chromatography to afford the title compound **5** as a colorless oil (500 mg, 0.94 mmol, 77%).

^{1}H NMR (400 MHz, $CDCl_3$, δ ppm): 5.24 (s, 1H, (NH)), 4.13 (d, 2H), 3.64- 3.51 (m, 24H), 3.35 (m, 2H), 2.50 – 2.47 (t, 2H), 2.28 – 2.21 (m, 6H), 1.59 – 1.56 (m, 2H), 1.43 (s, 9H), 1.35 (t, 1H), 0.95 – 0.90 (t, 2H).

^{13}C NMR (100 MHz, $CDCl_3$, δ ppm): 170.9, 98.8, 80.5, 70.6 – 70.1 (6C), 66.9, 62.7, 40.8, 36.3, 29.1, 28.1, 21.5, 20.1, 17.8.

1-[({bicyclo[6.1.0]non-4-yn-9-ylmethoxy}carbonyl)amino] 3,6,9,12,15,18-hexaoxahenicosan-21-oic acid 6

To a solution of *tert*-butyl 1-(bicyclo[6.1.0]non-4-yn-9-yl)-3-oxo-2,7,10,13,16,19,22-heptaoxa-4-azapentacosan-25-oate **5** (1 equiv., 500 mg, 0.854 mmol) in MeOH/H_2O 1/1 (10 mL) was added LiOH (10 equiv., 204 mg, 8.54 mmol). The reaction was stirred at room temperature overnight under argon atmosphere. After concentration, a solution of NaH_2PO_4 (1M, 50 mL) was added and the mixture was extracted with DCM (4 x 75 mL). The combined organic layers were washed with brine (75 mL), dried over $MgSO_4$ and concentrated *in vacuo* to afford the title compound **6** as a yellowish oil (400 mg, 0.75 mmol, 88%).

^{1}H NMR (400 MHz, $CDCl_3$, δ ppm): 5.35 (s, 1H (NH)), 4.14 (d, 2H), 3.79 – 3.76 (m, 2H), 3.67 – 3.64 (m, 20H), 3.57 – 3.54 (t, 2H), 3.35 (m, 2H), 2.62 – 2.59 (t, 2H), 2.29 – 2.19 (m, 6H), 1.58 (m, 2H), 1.37 – 1.33 (m, 1H), 0.96 – 0.91 (t, 2H).

^{13}C NMR (100 MHz, $CDCl_3$, δ ppm): 170.7, 98.9, 80.4, 70.6 – 70.2 (6C), 67.0, 62.8, 40.7, 36.4, 29.0, 21.5, 20.1, 17.8.

perfluorophenyl 1-((1R,8S,9s)-bicyclo[6.1.0]non-4-yn-9-yl)-3-oxo-2,7,10,13,16,19,22-heptaoxa-4-azapentacosan-25-oate 7

To a solution of 1-[({bicyclo[6.1.0]non-4-yn-9-ylmethoxy}carbonyl)amino] 3,6,9,12,15,18-hexaoxahenicosan-21-oic acid **6** (1 equiv., 650 mg, 1.23 mmol) and EDCI (2 equiv., 381 mg, 0.434 mL, 2.45 mmol) in dichloromethane (15 mL) was added pentafluorophenol (2 equiv., 451 mg, 0.257 mL, 2.45 mmol). The reaction mixture was stirred at room temperature for 4 hours under argon atmosphere. After concentration, the crude was dissolved in EtOAc (75 mL), washed with aqueous solutions of HCl (0.1 M, 75 mL) and saturated $NaHCO_3$ (2 x 75 mL). The combined organic layers were washed with brine (75 mL), dried over $MgSO_4$ and concentrated *in vacuo*. The residue was purified by flash chromatography (Cyclohexane/EtOAc 5/5 to EtOAc 100% in 20 minutes then EtOAc 100% to EtOAc/MeOH 95/5 in 10 minutes) to afford BCN-PEG_6-PFP **7** as a colorless oil (550 mg, 64%).

^{1}H NMR (400 MHz, $CDCl_3$, δ ppm): 5.19 (s, 1H (NH)), 4.06 (d, 2H), 3.82 – 3.80 (t, 2H), 3.59 – 3.56 (m, 20H), 3.50 – 3.48 (t, 2H), 3.31 (m, 2H), 2.89 – 2.87 (t, 2H), 2.22 – 2.13 (m, 6H), 1.53 – 1.50 (m, 2H), 1.30 – 1.27 (m, 1H), 1.21 – 1.18 (m, 2H), 0.89 – 0.85 (m, 2H).

^{13}C NMR (100 MHz, $CDCl_3$, δ ppm): 170.7, 98.8, 70.7 – 70.5 (4C), 70.3, 70.1, 66.1, 62.7, 53.4, 40.8, 34.4, 29.1, 21.4, 20.1, 17.8.

^{19}F NMR (400 MHz, $CDCl_3$, δ ppm): -157.55, -157.95, -162.33.

4-azidobenzoyl fluoride 8

The compound was synthesized from an adapted protocol, using TFFH instead of cyanuric fluoride.[1] TFFH (1.5 equiv., 242 mg, 0.919 mmol) and 4-azidobenzoic acid (1 equiv., 100 mg, 0.613 mmol) were dissolved in acetonitrile (5 mL) and DIPEA (1 equiv., 79.2 mg, 0.101 mL, 0.613 mmol) was added. The mixture was stirred at room temperature for 3 hours in the dark. The reaction mixture was poured onto ice water (20 mL) and diluted with diethyl ether (50 mL). The aqueous layer was discarded, and the organic layer was washed with water (2 x 10 mL) and brine (10 mL). The organic layer was dried over MgSO4, filtered and concentrated under reduced pressure to provide the crude residue, which was purified by silica pad (Cyclohexane) and lyophilized to afford the title compound **8** (64.8 mg, 0.392 mmol, 64 %) as a yellow solid.

Synthesis of BCN-siRNA conjugates

One aliquot of 3'-amino-RNA (1 equiv., 5 mM in RNase-free water) was diluted in RNase-free borate buffer (0.1 M, pH = 8.0) to 1.67 mM and BCN-PEG_6-PFP (50 equiv., 100 mM in DMSO) was added. The solution was topped-up with DMSO to 20% v/v. The mixture was incubated at 25°C for 4 hours under nitrogen atmosphere. An aqueous solution of $LiClO_4$ (3 M, 20 μL) was added and acetone cooled at -20°C was added (three times the total volume). The mixture was left at -20°C for 1 h to allow the oligonucleotide's precipitation. The mixture was centrifugated at 15000 g for 12 min and the supernatant was thrown away. This RNA precipitation step was done one more time. 3'-BCN-asRNA was dried in a speedvac and then dissolved in RNase-free PBS 1X (100 μL) and the concentration was measured by spectrophotometry using Nanodrop at 260 nm. Yield was between 55 and 84% depending on carefulness and scale.

To the solution of 3'-BCN-asRNA (1 equiv.) was added a solution of the complementary RNA strand (1.5 equiv. in RNase-free PBS 1X) and the solution was incubated at 65°C for 5 min, then the temperature was cooled from 65°C to 25°C over 15 min. BCN-siRNA was directly used for bioconjugation to antibody-N_3 without further purification.

mAb-N3 synthesis

To a solution of EphA2-antibody (1 equiv., 5 mg/ml in DPBS 1X, pH 7.4) was added azidobenzoyl fluoride (3 equiv., 20 mM in DMSO, fresh solution) and the mixture was incubated at 37°C for 30 min. Excess of reagent was removed by gel filtration chromatography using Bio-spin P-30 columns (Bio-Rad, Hercules, U.S.A.) pre-equilibrated with DPBS 1X (pH 7.4) to give a solution of mAb-N_3 (average yield 90%). The concentration was measured by spectrophotometry using Nanodrop at 280 nm and DoC was determined by SEC-ESI-MS.

mAb-siRNA synthesis

To a solution of mAb-N_3 (1 equiv., 10 mg/mL in DPBS 1x pH = 7.4) was added BCN-modified siRNAs (3 equiv., as a 100 μM solution in RNAse-free water) and the reaction mixture was incubated at 25°C for 24 hours.

The mixture was purified by size exclusion chromatography (Akta, Superdex 200 10/300 GL Increase, DPBS 1X as eluent). This method is efficient to separate the conjugated antibody from the naked one, therefore eliminating DoC 0 and free siRNAs. Fractions containing the product were concentrated by centrifugation (Vivaspin 500 μL, 50 kDa MWCO, 12 minutes, 15 000 g) and filtered through centrifuge tube filters (Corning® Costar® Spin-X®, 0.22 μm, 1 minute, 15 000 g). Average yield was between 30 and 40%. Protein concentration was determined by BCA assay, and 25 μg of conjugate were deglycosylated with Remove-iT® Endo S (New England Biolabs, Ipswich, U.S.A., Ref. P0741L) at 37°C for 2 hours before SEC-ESI-MS analysis.

Dual-labelled-mAb-siRNA conjugate synthesis for confocal microscopy

To a solution of mAb-N_3 (1 equiv., 10 mg/mL in DPBS 1x (pH 7.4)) was added Cy_3-BCN-siRNAs (3 equiv., as a 100 μM solution in RNAse-free water) and the reaction mixture was incubated at 25°C for 24 hours.

After purification by SEC to discard of unconjugated antibody, Cy_5-NHS ester (3 equiv., 16 h, DPBS 1X) was added to the purified mAb-siRNA. The use of Sulfo-Cy_5 led to high aggregation of the final conjugate. Excess of reagent was removed by gel filtration chromatography using Bio-spin P-30 columns (Bio-Rad, Hercules, U.S.A.) pre-equilibrated with DPBS 1X (pH 7.4) to afford the dual-labelled antibody (yield 12% over two steps). Prior to biological assay, the conjugate was filtered through centrifuge tube filters (Corning® Costar® Spin-X®, 0.22 μm, 1 minute, 15 000 g) for sterilization. Protein concentration was determined by BCA assay.

Biological assays

Cell culture for confocal microscopy

The day before experiment, A549-Dual cells (4000 cells/well, 25 μL) were plated in a 384-well flat-bottomed black plate suitable for microscopy in DMEM complete medium without phenol red. Conjugates were diluted to 1 μM in Opti-MEM (Thermo Fisher Scientific, Ref. 31985062), and cells were then treated with 100 nM of conjugates. After 1 h and 4 h, cells were washed with DPBS 1X, resuspended in DMEM complete medium without phenol red, and labelled with 5 μg/mL Hoechst 33342 (ThermoFisher, Ref. 62249) and Lysoview 488 (Biotium, Ref. 70067, dilution 1/1000 in complete medium) 30 minutes before the reading. After these 30 minutes, cells were washed with DPBS 1X and pictures were taken on a Zeiss LSM800. Images were analyzed by ImageJ, background and colors were normalized and Pearson's correlation coefficient was determined with the plugin coloc 2.

RIG-I activation assays and viability assay

The day before experiments, 10,000 A549-Dual or A549-Dual RIG-I KO cells were plated in a flat-bottomed transparent 96-well plate in 90 μL DMEM complete medium. Antibodies were diluted to 400 nM in Opti-MEM (Thermo Fisher Scientific, Ref. 31985062). All siRNAs were diluted to 400 nM in Opti-MEM containing LipofectamineTM RNAiMAX (Thermo Fisher Scientific, Ref. 13778075) for 5 minutes according to manufacturer's protocol. Then, 10 μL of these solutions were added to cells.

For EphA2-dependent internalization assay, cells were pre-incubated with increasing concentration of the naked antibody for 1 hours in order to degrade surface-EphA2, then washed with DPBS 1X before adding the antibody-siRNA conjugates for 72 h.

Luciferase assay (Quanti-LucTM Gold, Invivogen, Ref. rep-qlcg5) was performed in a 96-well flat-bottomed white plate according to the manufacturer's protocol.

SEAP assay (Quanti-BlueTM, invivogen, Ref. rep-qbs) was performed in a 96-well flat-bottomed transparent plate according to the manufacturer's protocol.

WST-1 assay (Roche, Merck, Ref. 11644807001) was performed according to the manufacturers' protocol.

Western-blot

The day before experiment, A549-Dual cells (400,000 cells/well, 1.8 mL of DMEM complete medium) were plated in a flat-bottomed transparent 6-well plate. All compounds were diluted to 400 nM with Opti-MEM and 200 µL of these solutions were added to the wells, and cells were incubated for 72h.

Cells were washed with DPBS, harvested using a scrapper, then 200 µL of freshly prepared RIPA buffer (containing 50 mM Tris-HCl pH = 7.4, 150 mM NaCl, 1% NP-40, 1 mM PMSF, protease and phosphatase inhibitor cocktail 1X (Thermo Fisher Scientific, Ref. 78442)) was added. Cells were then sonicated (3 x 10 sec), centrifugated at 13,000 g for 10 min and let rest for 15 min over ice.

Total protein level of the supernatant was measured by BCA assay (BSA 1 mg/mL as standard) and 50 µg of cell proteins were loaded in a 4-15% precast Stain-Free SDS-PAGE gel (Bio-Rad, Ref. 4568084, 200V, 40 min, weight marker All Blue standard). Gels were then transferred into nitrocellulose membranes (Bio-Rad, Ref. 1704158) using Trans-Blot Turbo Transfer System (Bio-Rad). Membranes were put in a box containing 10 mL of blocking buffer (5% milk in TBS-T 1X (Tris-base 20 mM, 13,6 mM NaCl, pH adjusted with HCl to 7.6, tween 20 0.1%) for 1h. After washing with TBS-T 1X (3 x 5 min), 10 mL of primary antibodies solution (mouse mAb anti-PLK1 (Abcam, Ref. ab17056), rabbit pAb anti-RIG-I (Cell Signal, Ref. 3743S), both at 1 µg/mL (dilution 1/1000) in TBS-T 1X containing 5% BSA) was added overnight at 4°C. For internalization assay, goat mAb anti-human-Fc (Merck, Ref. I2136) was used in the same conditions.

After washing with TBS-T 1X (3 x 5 min), 10 mL of primary antibody solution (mouse mAb anti-GAPDH (invitrogen, Ref. MA5-15738) at 1 µg/mL (dilution 1/1000) in TBS-T 1X containing 5% BSA) was added for 45 minutes at room temperature. After washing with TBS-T 1X (3 x 5 min), 10 mL of secondary antibodies solution (donkey mAb anti-mouse and horse mAb anti-rabbit, both HRP conjugates, at 0.2 mg/mL (dilution 1/5000) in TBS-T 1X containing 5% BSA) were added for 2 hours at room temperature. After washing with TBS-T 1X (3 x 5 min), nitrocellulose membrane was revealed with SuperSignal (Thermo Fisher Scientific, Ref., 34580) according to manufacturer's protocol and ChemiDoc (Bio-Rad). Blots were quantified using Image Lab (Bio-Rad) and results were normalized to GAPDH.

Cell cycle study

The day before experiments, 10,000 A549-Dual cells were plated in a flat-bottomed transparent 96-well plate in 90 µL DMEM complete medium. Nocodazole (500 nM in Opti-MEM) was used as a G2/M synchronizer product to place cytometry gates. Antibodies were diluted to 400 nM in Opti-MEM (Thermo Fisher Scientific, Ref. 31985062). All siRNAs were diluted to 400 nM in Opti-MEM containing LipofectamineTM RNAiMAX (Thermo Fisher Scientific, Ref. 13778075) for 5 minutes according to manufacturer's protocol. Then, 10 µL of these solutions were added to cells before performing the assay after 24h of incubation.

After 24 h of incubation, cells were washed with DPBS 1X (50 µL/well) and accutase was added (50 µL/well) to detach cells. After 5 min of incubation at 37°C, the plate was shaken to detach cells. 20 µL of each well was transferred into a V-bottomed black 96-well plate and 20 µL of MultiCyt Cell Cycle Screening Kit (Sartorius, diluted in FACS buffer, 1:50) was added to each well. After incubation in the dark for 1 hour at room temperature, data were collected with an iQue Screener PLUS using the given template and ForeCyt software.

Calreticulin exposition assay

The day before experiments, 10,000 A549-Dual cells were plated in a flat-bottomed transparent 96-well plate in 90 µL DMEM complete medium. Antibodies were diluted to 1 µM in Opti-MEM (Thermo Fisher Scientific, Ref. 31985062). All siRNAs were diluted to 1 µM in Opti-MEM containing LipofectamineTM RNAiMAX (Thermo Fisher Scientific, Ref. 13778075) for 5 minutes according to manufacturer's protocol. Then, 10 µL of these solutions were added to cells before performing the assay after 48 h of incubation.

Cells were washed with DPBS 1X (50 µL/well) and detached using accutase (50 µL/well) and incubated for 10 min at 37°C. Cells were then transferred into a 96-well V-bottomed black plate, centrifuged (200 g, 5 min), and washed once with FACS buffer (PBS, 2% BSA, 10 mM EDTA, centrifuge 200 g, 5 min). Cells were resuspended in FACS buffer, and AF488-tagged anti-CALR mAb (Abcam, Ref. ab196158, dilution 1/100, 50 µL) was added and incubated for 30 minutes at 4°C in the dark. Cells were washed with FACS buffer (200 g, 5 min) and resuspended in FACS buffer (100 µL). Then, 1 µL of 7-AAD (Miltenyi Biotec, Ref. 130-111-568) was added in each well. Data were collected with Miltenyi Biotec's MACS Quant 10 and data were analyzed with FlowJo software.

Killing assays

In prevision of co-culture experiments with PBMCs, A549-Dual or A549-Dual RIG-I KO cells were cultured in RPMI 1640 containing 1% GlutaMAXTM (GibcoTM, ThermoFisher, Ref. 61870036) and supplemented with 10 µg/mL Blasticidin (InvivoGen, Ref. ant-bl-05), 100 µg/mL Zeocin (InvivoGen, Ref. ant-zn-05), 10% v/v heat inactivated Fetal Bovine Serum (FBS, GibcoTM, ThermoFisher, Ref. 10099141). The day before experiment, A549 cells (2500 cells/well, 50 µL in RPMI 1640 complete medium) were plated on a 96-well flat-bottomed black plate suitable for microscopy. The same day, PBMCs were thawed, washed twice with DPBS 1X (centrifuged at 300 g for 8 min) and incubated overnight in RPMI 1640 complete medium.

The next day, PBMCs were washed one more time and counted just before seeding in the A549 cell-containing plates (25 μL, ratio A549/PBMC = 1/5). Antibodies or Resiquimod (TLR7/8 agonist, Invivogen, Ref. tlrl-r848) were added (25 μL, RPMI 1640) to each well, and Incucyte Caspase 3/7 Green dye (Sartorius, Ref. 4440) and Incucyte Annexin V Red dye (Sartorius, Ref. 4641) were added according to manufacturer's protocol. Cells were incubated in Incucyte S3 Live Cell Imaging System (Sartorius). Images were taken every 2 hours for 4 days and analyzed using Incucyte's software. The supernatant of each plate was used for cytokine quantification.

Cytokine quantification

Each cytokine was quantified using iQue Qbeads personalized PlexScreen (Sartorius) according to manufacturer's protocol D (one-wash protocol + standard curves). Rapidly, 10 μL of supernatant were transferred to a black V-bottomed 96-well plate, and 10 μL of Qbeads were added for 1 h at room temperature. Following this incubation, 10 μL of secondary antibodies were added for 2 hours at room temperature, and then the cytokines were quantified using IQue Screener PLUS using the given template and ForeCyt software.

QUANTIFICATION AND STATISTICAL ANALYSIS

Statistical analysis was performed using the GraphPad Prism Software version 9.0.0. All the values for the *in vitro* experiments were done are presented as mean ± SD from one of at least three separate experiments. Significant differences (p value) were discriminated by applying a two-tailed, unpaired Student's t test assuming a normal distribution. p values are indicated in the corresponding figures.